List of abbreviations

ABV	Adriamycin, bleomycin and vincristine
Alx647	Alexa Fluor® 647 azide
^{13}C NMR	Carbon-13 nuclear magnetic resonance
CMC	Critical micelle concentration
$CHCl_2$	Dichloromethane
$CHCl_3$	Trichloromethane, chlorophorm
cryo-TEM	Cryogenic transmission electron microscopy
CTA	Chain transfer agent
DCC	*N*,*N*′-Dicyclohexylcarbodiimide
DDS	Drug delivery systems
DDD	Drug delivery devices
DHAD	Dihydroxyanthracenedione
DLD1	Colorectal adenocarcinoma
DMAC	Dimethylacetamide
DMAP	4-(Dimethylamino)pyridine
DMF	Dimethylformamide
DMSO	Dimethyl sulfoxide
DNA	Deoxyribonucleic acid
DLS	Dynamic light scattering
DPA	2-(Diisopropylamino)ethyl methacrylate
Dox	Doxorubicin
Dtxl	Docetaxel
e.g	Used to provide an example
EGFR	Epidermal growth factor receptor
ELS	Electrophoretic light scattering
EPR	Enhanced Permeability and Retention
EtOH	Ethanol
Et_3N	Triethylamine
FDA	Food and Drug Administration
FC	Flow cytometry
FLIM	Fluorescence lifetime imaging microscopy
FR	Folate receptors
FT-IR	Fourier transfomed infrared spectroscoy
^{1}H NMR	Proton nuclear magnetic resonance spectroscopy
H_2O	water
H_2O_2	Hydrogen peroxide
HPLC	High-performance liquid chromatography
HeLa	Human cervical carcinoma
HF	Human fibroblast
HPMA	(*N*-(2-hydroxypropyl)methacrylamide)
i.a	inert atmosphere
i.e	Used to offer more information
mABs	Monoclonal antibodies
NSCLC	Non-small cell lung cancer
NPs	Nanoparticles
NGR	Asparagine-glycine-arginine
NR	Nile Red

NTA	Nanoparticle tracking analysis
PAA	Poly(aspartic acid)
PACA	Polyalkylcyanocrylate
PBCA	Polybutylcyanocrylate
PBS	Phosphate buffer saline
PBSBDL	Poly(butylene succinate-*co*-butylene dilinoleate)
PCL	Polycaprolactone
PC3	Human prostate carcinoma
PDI	Polydispersity index
PDPA	Poly[2-(diisopropylamino)ethyl methacrylate]
PEG	Polyethylene glycol
PEO	Polyethylene oxide
pH_e	Extracellular pH
pH_i	Intracellular pH
PHPMA	Poly(*N*-(2-hydroxypropyl)methacrylamide)
PLA	Poly(lactic acid)
PLL	Poly(L-lysine)
PGA	Poly(L-glutamic acid)
PLGA	Poly(lactic-*co*-glycolic acid)
PRINT	Particle replication in nonwetting templates
PTX	Paclitaxel
PSMA	Prostate specific menbrane antigen
pTSA	P-Toluenesulfonic acid
PVA	Polyvinil alcohol
PVP	Poly(*N*-vinyl-2-pyrrolidone)
RAFT	Reversible addition-fragmentation chain transfer
RES	Reticuloendothelial system
RGD	Arginine-glycine-aspartate
ROP	Ring-opening polymerisation
ROS	Reactive oxygen species
RT	Room temperature
SAXS	Small-angle X-ray scattering
scFv	Single-chain variable fragment
SEC	Size-exclusion chromatography
SLS	Static light scattering
siRNA	Small interfering ribonucleic acid
TEM	Transmission electron microscopy
THF	Tetrahydrofurane
TPGS	D-α-tocopheryl polyethylene glycol succinate
VCR	Vincristine sulfate
WHO	World Health Organization

List of symbols

A	Absorbance
D_H	Hydrodynamic diameter
M_n	Number average molecular weight
M_w	Weight average molecular weight
n	Refractive index
R_G	Radius of gyration
R_H	Hydrodynamic radius
λ	Wavelength
Γ	Decay rate
μ_2	Second cumulant
k_B	Boltzamann constant
τ	Lifetime
ζ	Zeta potential
s	Solvent
$<$	Major
$>$	Minor
$\leq$	Minor or equal
$\geqq$	Major or equal
$\sim$	Around
I_s	Scattering intensity
d_n/d_c	Refractive index increment
R_θ	Rayleigh ratio
θ	Angle

1. Aims of the thesis

Cancer is a leading cause of death throughout the world (WHO) being responsible for 84 million of deaths between 2005 and 2015 making the development of novel biomedical technologies/and or strategies to improve conventional chemotherapies of upmost importance. The central focus of current research is to increase the survival time and to enhance the patient quality-of-life. Unfortunately, for several treatments, only a limited dosage reaches the desired tumor site, resulting in ineffective responses, mainly due to the lack of tissue selectivity of the chemotherapeutic to the cancer site. Soft matter assemblies as nanotechnology based systems can reach the desired tumor site with higher drug amounts then their free drug counterparts. Based on this, emphasis is put here to the current investigations and potential novel approaches towards overcoming the remaining challenges in the field of chemotherapy through soft matter assemblies as well as to a brief overview of formulations that are in clinical trials and marketed products (successful cases). Taking into account higher levels of accumulation in tumors and based on the main advantages and drawbacks of each of the soft matter assemblies described, drug-loaded block copolymer micelles and biodegradable polymeric nanoparticles (non-responsive and responsive to external stimuli) were selected as soft matter systems to improve the conventional chemotherapies, and perhaps one day, enhance the patient quality-of-life committed with the cancer disease. These features are presented along this thesis.

2. Introduction

2.1 Cancer and nanomedicine

Cancer is a leading cause of death throughout the world. The WHO estimates that cancer caused and will cause the deaths of 84 million people between 2005 and 2015 [1]. Therefore, current investigations are focused on the discovery of novel, powerful anticarcinogenic compounds as well as the development of novel biomedical technologies to improve conventional therapies. The development of more effective therapies has become a multidisciplinary challenge incorporating materials science, biomedical engineering, life science and clinical practice. The central focus of current research is increasing survival time and enhancing patient quality-of-life. Conventional cancer treatments are currently based on chemotherapy. There are extremely powerful active agents marketed for clinical use, and due to the efficacy of the pharmacological compounds, tissue selectivity is of utmost importance. Unfortunately, for several treatments, a limited dosage reaches the desired tumor site, resulting in ineffective responses. Consequently, current research investigations are devoted to increasing the efficacy and selectivity of known chemotherapeutics rather than discovery of novel compounds. Therefore, it is important to understand tumor site pathophysiology and its distinct features compared with normal tissues. This knowledge is emerging as an alternative for overcoming the lack of specificity of conventional chemotherapeutic treatments. In the next subsection a brief description of the particular features of tumor microenvironments will be provided, with special consideration given to tumor vasculature and physicochemical properties.

2.1.1 Particular features of cancer sites

Tumor vasculature

The cardiovascular system is responsible for the removal of waste metabolites as well as the delivery of nutrients, oxygen, blood and immune cells to all organs and tissues. The cardiovascular system develops through the vasculogenesis and angiogenesis processes. In pathological states, such as cancer and chronic inflammation, the rapid development of tumor cells requires the generation of new blood vessels to supply the necessary amounts of oxygen and nutrients [2]. In such conditions, the vasculature can be abnormally and irregularly activated. Generally, the blood vessel growth is poorly-aligned and has wide fenestrations. Furthermore, tumor

tissues usually lack effective lymphatic drainage. Such structural differences compared with normal tissues modify fluid dynamics. The porosity and "leaky" vasculature enable the permeation and retention of macromolecular drugs and aggregates due to impaired lymphatic drainage within tumor sites. This phenomenon is known as the enhanced permeation and retention (EPR) effect. This enhanced retention is primarily caused by a lack of lymphatic vessels in the tissue surrounding tumor sites [3].

Physicochemical aspects

In addition to the particular features of tumor vasculature, tumor sites can be distinguished from normal tissues, largely characterized by their slightly acidic extracellular pH (pH_e) and interstitial pressure gradient. The extracellular pH of tumor sites is slightly below 7.4 due to a lack of oxygen. This is caused by an insufficient blood supply because new blood vessel generation is generally not sufficiently rapid during tumor expansion. This leads to a hypoxic state where the tumor locality is deprived of an adequate oxygen supply. The hypoxic condition is generally followed by the production of higher lactic acid amounts, which contribute to the formation of an acidic microenvironment [4]. The pH_e in tumor sites usually ranges from 6.0 to 6.8 depending on the tumor aggressiveness. Conversely, tumor cell intracellular pH (pH_i) is usually similar to values observed in normal tissues, ranging from 4.5 in lysosomes up to 8.0 in mitochondria [5, 6]. Due to the wide pH range from pH_e to pH_i, pH-responsive polymer-based supramolecular assemblies with pK_a 5.0-8.0 are susceptible to drastic changes in their physicochemical properties as a function of pH when travelling from the extracellular to intracellular microenvironments. This property is frequently considered during the development of pH-responsive systems [7-10].

Additionally, high interstitial fluid pressure is a typical feature of solid tumors. Generally, chemotherapeutics and high molecular weight nanocarriers are transferred from the bloodstream to tumor sites *via* convection, and the high interstitial fluid pressure of the tumor reduces the effectiveness of this process, which ultimately leads to a reduction of the uptake fraction of the active agent by the tumor site. Additionally, tumor sites generally maintain a negative interstitial pressure gradient, *i.e.*, the pressure in the tumor core is higher than the surrounding tissue. This property restricts the tumor's drug accumulation capacity because chemotherapeutics and high molecular weight nanocarriers will preferentially flow toward the low pressure region [11, 12].

2.1.2 Tumor accumulation of active drugs and nanoparticles

The protection of chemotherapeutics using nanoparticle technology avoids the rapid degradation of active agents. The use of nanoparticles also reduces side-effects and provides higher therapeutic efficacy, sustained drug release and potentially specific accumulation and increased blood circulation half-life [13]. The permeation of active agents and supramolecular delivery systems into tumor sites is facilitated by their specific aforementioned features. Tumor accumulation may be achieved by passive or active targeting depending on the surface properties of the nanocarrier. Truly active targeting can only occur after passive accumulation.

Passive targeting and the EPR effect

The blood vessels in solid tumors possess specific pathophysiological characteristics, such as extensive angiogenesis, irregular architecture with a discontinuous epithelium (hypervasculature), lack of a basal membrane, impaired lymphatic drainage and extensive production of numerous permeability mediators [11, 14]. Almost 30 years ago, two independent studies identified important principles for the selective accumulation of large molecules into tumors [15]. Firstly, the interesting fact that tumor vessels are hyperpermeable to large macromolecules compared with normal vessels [16], and secondly, the fact that large macromolecules can be retained within tumors due to poor clearance [17]. The tumor blood vessels are heterogeneous in their spatial distribution and are dilated, resulting in fenestrations in their capillaries. Depending on tumor type, these fenestrations can reach sizes from 10 nm to 2 μm [15, 18, 19]. Macromolecules and nanocarriers with appropriate dimensions (ranging from 10 to 200 nm) [20] are able to extravasate the large pores in the abnormal tumor vessels resulting in enhanced permeation. Additionally, lymphatic vessels are absent or non-functional in tumors, contributing to dysfunctional lymphatic drainage, resulting also in enhanced retention of permeated macromolecules. The extravasation, with enhanced permeation and retention of macromolecules, results in the mechanism known as the enhanced permeation and retention (EPR) effect, schematically depicted in Figure 1. This phenomenon has been, to date, the basis of nanotechnology platforms for active agent delivery to tumors [21].

The pioneering investigations on this issue were performed by Matsumura and Maeda [17, 22, 23]. These studies were based on biodistribution observations of protein-polymer conjugates (SMANCS), chemical conjugates with a synthetic copolymer of styrene-*co*-maleic acid (SMA) and various radioactive (^{51}Cr-labeled)

proteins of various molecular sizes (12 kDa - 160 kDa). The investigators observed a considerable time-dependent accumulation of SMANCS and plasma proteins with molecular weight greater than 60 kDa [17]. Furthermore, after an injection of a labeled albumin-dye complex (69 kDa), macromolecule accumulation was observed in normal and tumor tissues, with the retention of the complex only observed in tumor tissues.

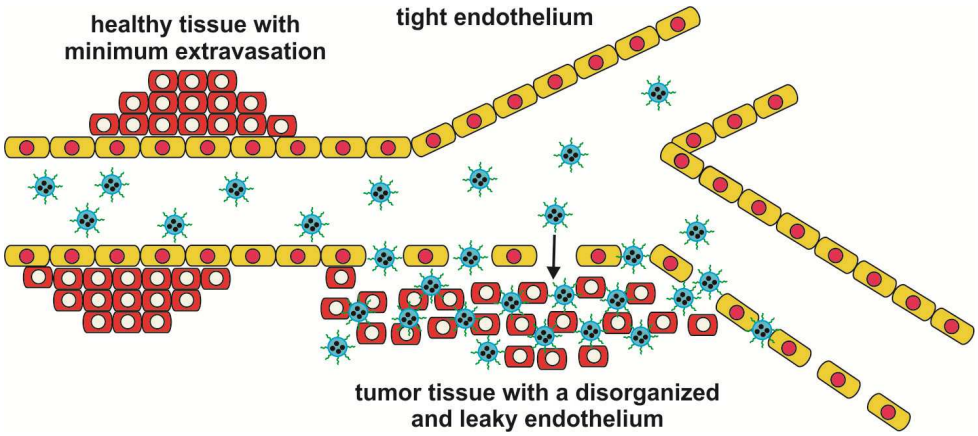

Figure 1. Schematic representation of passive tumor nanoparticle accumulation due to the enhanced permeation and retention (EPR) effect.

This unique phenomenon of accumulation in solid tumors is considered a landmark for vectoring chemotherapeutics to tumors. Because these peculiarities are not observed in normal tissues, the discovery of the EPR effect is becoming a promising strategy for the further development of cancer therapies. As a result of the particular anatomical characteristics and pathophysiology of tumor tissues, the concentration of macromolecules and nanocarriers can reach values up to one hundred times higher than the concentration in normal tissues [17, 21, 23, 24]. Nevertheless, it is worth emphasizing that the EPR effect is a highly heterogeneous phenomenon, which can be substantially different from tumor to tumor and from patient to patient [11, 25, 26]. This effect is also time-dependent during treatment [27, 28], which has limited the progress of the development of therapies based on the EPR concept to date [29].

Active targeting and surface functionalization

The term “active targeting” is generally related to the surface functionalization of nanoparticles with targeting ligands to allow binding to specific receptors overexpressed by tumor cells, tumor vasculature or tumor

tissues [20, 25, 30]. Active targeting is also called ligand-mediated targeting and is usually implemented to favor target cell recognition and target cell uptake. Therefore, it does not aim to improve overall tumor accumulation [31, 32]. Ligand-mediated targeting is particularly useful for the intracellular delivery of active agents unable to cross cellular membranes by themselves, such as siRNA and plasmid DNA [33-35]. Ideally, the receptors must be expressed homogeneously in all target cells, and the active-target nanoparticle must be in the tumor vicinity to enhance affinity [31, 36]. The nanoparticle binding affinity is dependent on the nanoparticle architecture, ligand specificity and ligand chemistry [30]. Physicochemical properties, such as size, shape and ligand density, may also possibly affect the efficacy of the active targeting strategy [37, 38].

The nanoparticle internalization is frequently important to increase the efficacy of antitumor agent delivery. The ligand nature is also important with regard to the mechanism of cell uptake. Long circulation times allow effective transport of the nanoparticles to tumor sites and nanoparticle accumulation *via* the EPR effect. Subsequently, specific ligands may contribute to an efficient endocytosis process. Effective internalization of nanoparticles generally leads to an increase in the therapeutic effect [39, 40].

Antibodies (monoclonal antibodies - mAbs or antibody fragments - scFv), proteins, peptides and other molecules, such as nucleic acids, carbohydrates, folate and aptamers, are amongst the most investigated ligands for nanoparticle surface functionalization (Figure 2, left). These categories are described individually in detail in the Appendix of the thesis (*vide* **publication 1**).

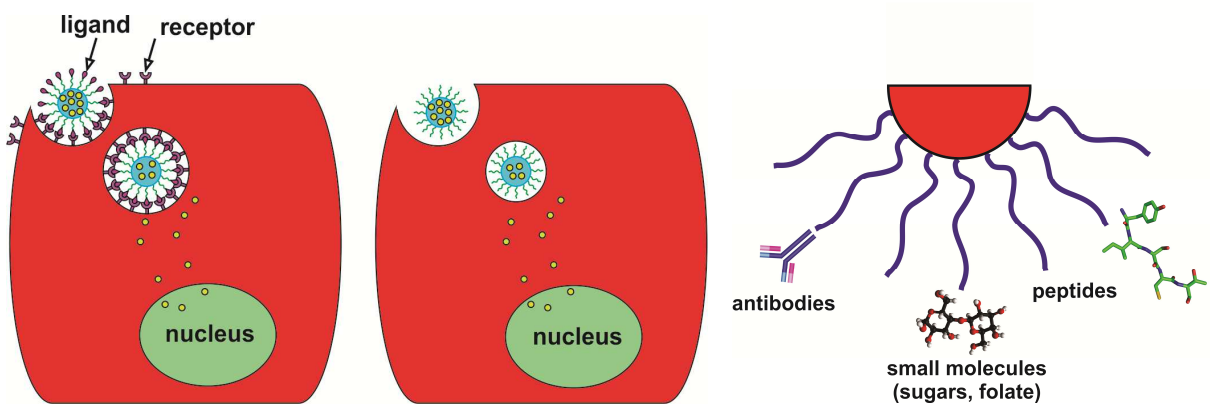

Figure 2. Schematic representation of cell internalization by endocytosis *via* ligand-mediated targeting (left) and *via* passive targeting (middle). Schematic representation of commonly used targeting ligands for nanoparticle surface functionalization (right).

Intracellular Delivery of Active Agents

Intracellular delivery is required for the therapeutic activity of macromolecules (particularly large and charged molecules, *i.e.*, siRNA, peptides) that cannot enter cells independently [20, 25]. Internalization can be mediated by the incorporation of different molecular classes onto the nanoparticle surface as described above. Ideally, nanomedicines must be able to deliver therapeutic agents into the target cells with minimal cytotoxicity. Subsequent to tumor accumulation and cell internalization, encapsulated therapeutic agents must be released into the pre-nuclear region of damaged cells. This drug release may occur *via* a slow diffusion process or, preferably, *via* an external stimuli or change in environmental condition, such as pH [42]. As previously mentioned, the pH of normal tissues (pH ~ 7.4) is progressively reduced to values near 6.5 - 6.0 in the extracellular region of tumor sites. High molecular weight nanocarriers are generally cell-internalized *via* endocytosis and during this process early endosomes gradually mature into late endosomes and eventually lysosomes [43]. Therefore, it is essential that the encapsulated therapeutic is released prior to lysosome formation, where the drug may be degraded. Endosome maturation is linked to a drastic reduction of the internal organelle pH to ~ 5.0. Therefore, polymer-based pH-responsive materials, which are susceptible to destabilization in acidic conditions, can ideally circulate in the slightly basic bloodstream and undergo further disintegration in the acidic organelle environment. Polymers containing amino groups with pKa ~ 5.0 - 7.4 demonstrate this behavior. The reduction in environmental pH may favor fast drug release, avoiding potential drug degradation. Endosomal escape is the

most accepted mechanism for explaining the release of macromolecular drugs and high molecular weight nanocarriers from late endosomes due to the proton sponge effect, as outlined in Figure 3.

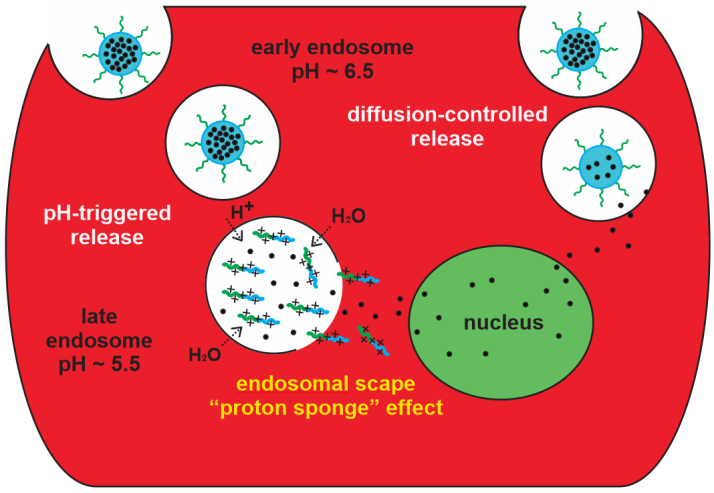

Figure 3. Schematic representation of the intracellular delivery of active agents *via* diffusion-controlled (right) and pH-triggered (left) mechanisms.

During the proton sponge effect, agents that can be protonated subsidize the ionic concentration increase inside the organelles, stimulating osmotic swelling of late endosomes causing further membrane rupturing and content release prior to its degradation. Polymers with amine groups have been demonstrated to be efficient for the intracellular delivery of active agents and genes due to protonation in acidic environments [44].

2.2 Classes of soft matter based nanomedicines for cancer therapy

Soft materials are generally susceptible to environmental conditions. Polymer-based nanomedicines can carry, either covalently linked or physically entrapped, an enormous variety of active agents, including drugs, contrast probes, proteins and nucleic acids. Therefore, they can be potentially employed in numerous biomedical applications. Specifically, polymeric assemblies have received substantial attention due to their versatility and "smartness", as their structure can be modified *via* external stimuli (temperature, pH, light), allowing nanomedicines to be loaded with and deliver active molecules and contrast agents in a controlled fashion and, ideally, to desired sites.

Current investigations into the updated definition of soft matter based nanomedicines were begun decades ago by the convergence of polymer chemistry, materials engineering, biology and pharmacology. This

convergence led to the development of numerous nanomedicines, including, initially, liposomes, followed by polymer-drug conjugates, drug-loaded block copolymer micelles and biodegradable polymeric nanoparticles. In this section, I will describe the most investigated classes of soft matter based nanomedicines and recent advances that have focused on cancer chemotherapy.

2.2.1. Liposomes

Liposomes are self-assembled, swollen vesicular nanostructures produced from amphiphilic phospholipids. The pioneers in the field described these swollen phospholipid systems in 1965 [45], initially naming them bangosomes. These structures were later conceptually established as drug delivery systems and were referred to as liposomes [46]. Liposomal nanostructures have a hydrophilic inner compartment, which made them suitable for hydrophilic cargo, such as DNA and therapeutic proteins [47, 48]. Moreover, hydrophobic agents can be entrapped within the hydrophobic region of the membrane such as schematically represented in Figure 4. However, the loading capacity is limited and sometimes results in unstable entities [49].

Liposomes can be tailored to deliver cargo using a diverse library of lipids that have specific biophysical behaviors [48-50]. The self-assembly can be controlled by lipid selection, providing control over liposome morphology and structure as well as biophysical characteristics. The lipids can be synthetically designed or naturally occurring compounds. Therefore, researchers can select a variety of hydrophilic head groups, specific linkers and hydrophobic moieties [51]. The development of liposomes has led to advances in the nanomedicine field. Many biomedical areas have been covered by liposomal research, including the delivery of drugs, vaccines, imaging and contrast agents [48, 49]. The control of drug-loading, liposome size, the preparation of long-circulating liposomes (PEGylated), triggered release liposomes (by light, heat, pH, ultrasound), ligand-mediated targeted liposomes and liposomes used to co-deliver drugs have been recently reviewed [48, 51].

Among the investigated nanomedicines, liposomes were the first to transition from concept to clinical application and they are now an established technology platform that has considerable clinical acceptance, with several FDA approved formulations for cancer chemotherapy. To date (August 24th, 2015), 13 clinically approved liposome agents that generate over $750 million in revenue (2011) are on the market [50].

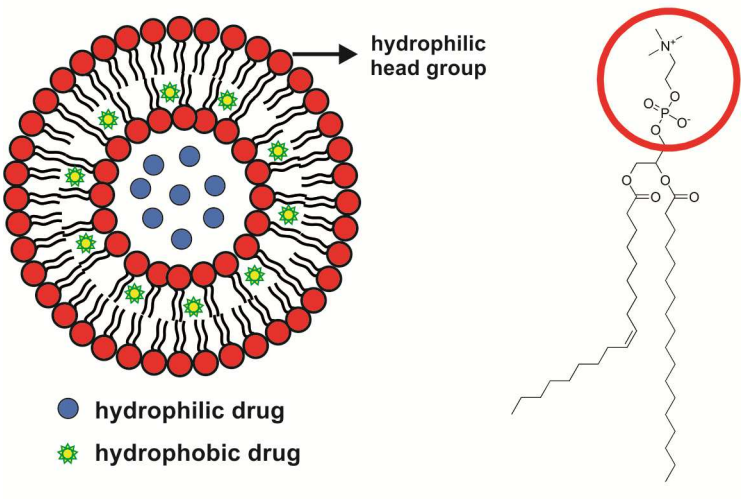

Figure 4. Schematic representation of a drug-loaded liposome (left) and the molecular structure of a phosphatidylcholine related phospholipid (right**).**

2.2.2. Biodegradable polymeric nanoparticles

Biodegradable polymeric nanoparticles comprise primarily nanospheres and nanocapsules. They are generally employed to deliver hydrophobic active agents that can be dissolved within the oily core of nanocapsules that is surrounded by a polymeric wall or uniformly distributed in the polymeric nanosphere matrix (Figure 5) [52].

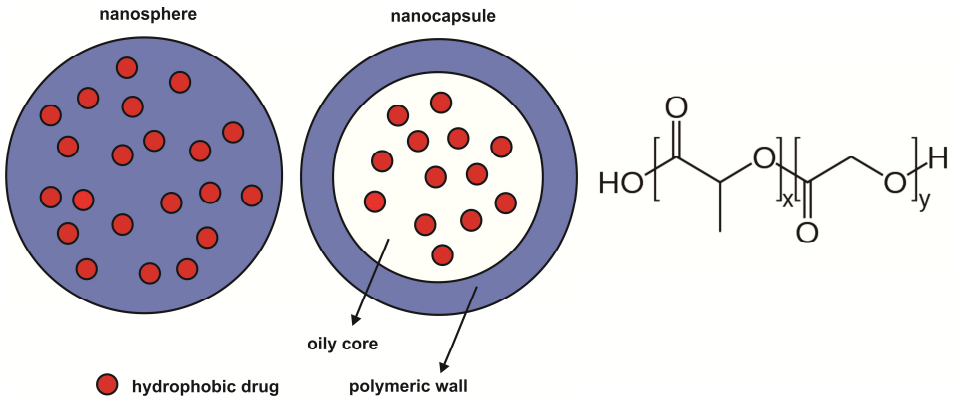

Figure 5. Schematic representation of a drug-loaded nanosphere (left) and nanocapsule (middle). The molecular structure of PLGA, a widely used biodegradable polymer for biodegradable polymeric nanoparticle production, is also portrayed (right).

Biodegradable polymeric nanoparticles were initially reported a few years after liposomes [53] and they have also attracted considerable attention for improving conventional chemotherapies. The development of biodegradable polymeric nanoparticles has rapidly emerged along to establishing methods for the industrial production of polyalkylcyanoacrylate (PACA) [54], poly(lactic acid) (PLA) [55], poly-ε-caprolactone (PCL) [56], poly(lactic-*co*-glycolic acid) (PLGA) [57] and chitosan [58]. Currently, the most investigated systems are manufactured from FDA approved biodegradable polymers, including PLA, PCL and PLGA. The advantage of these polymers is that they are degraded into smaller, biocompatible molecules that are easily cleared *via* conventional paths, such as renal and hepatic filtration [59]. Nanoparticles made by PLGA and PLA are frequently employed to encapsulate anticancer drugs. The biodegradable polyester nanoparticles are generally produced using nanoprecipitation (solvent-shifting) [60] or emulsion-evaporation [61] methods. Recently, more refined techniques have also been used for biodegradable nanoparticle production, such as continuous-flow microfluidics [62] or PRINT (particle replication in nonwetting templates) [63]. Notably, the PRINT process appears to circumvent two of the major remaining difficulties in the polymeric nanoparticles field: low encapsulation efficiency of active agents and control over particle size and dispersity. Studies have demonstrated that PLGA nanoparticles manufactured using the PRINT approach are uniformly distributed with high and efficient loadings of docetaxel (40% *w*/*w* with encapsulation efficiency higher than 90%) [64] and have proven beneficial *in vivo*.[65] Currently, there are reports of PLA and PLGA nanoparticles loaded with several antitumor agents, including paclitaxel, docetaxel and cisplatin [66, 67].

Furthermore, the development of new biodegradable polymers, as alternatives to the aforementioned FDA approved polyesters, has also attracted considerable attention. Recently, there have been reports that the acylation of poly(glycerol adipate) with fatty acids (laurate, stearate and behenate) generates new amphiphilic biodegradable polymers with promising properties for nanoparticulate drug carrier systems [68]. We have recently reported the synthesis and characterization of a new aliphatic biodegradable-based fatty acid copolyester named poly(butylene succinate-*co*-butylene dilinoleate) (PBSBDL). Surfactant-free 6-7% $w_{drug}/w_{polymer}$ paclitaxel-loaded nanoparticles (~ 120 nm) that had pronounced stability and relatively rapid degradation were obtained. Cell viability experiments demonstrated that the nanoparticles are fully biocompatible and non-toxic, making them potentially useful for biomedical applications [69].

Nevertheless, despite the favorable biocompatibility of polyester nanoparticles, their largest issue is rapid uptake and clearance immediately after injection unless a stabilizer is used. To circumvent this difficulty, NPs are generally produced with a stabilizing outer shell, generally achieved by grafting, conjugating or

adsorbing highly hydrophilic polymers, such as poly(ethylene glycol) (PEG), polysaccharides (usually dextran or chitosan), polyvinyl alcohol (PVA) or poly(*N*-vinyl-2-pyrrolidone) (PVP). However, although they display excellent non-bioadhesive properties, the aforementioned hydrophilic polymers have specific weaknesses and limitations when used for long-term applications: the polysaccharides are strong activators of the complement system [70], PVA can reduce uptake and sometimes must be avoided due to associated toxicity [71, 72], while PEG and PVP may undergo oxidative degradation [73, 74]. Considerable efforts have been directed towards the development of alternative bioinert polymers to improve the blood circulation time of nanomedicines [75]. Accordingly, PLGA nanoparticles comprising D-α-tocopheryl polyethylene glycol succinate (TPGS) as an emulsifier/surfactant to deliver paclitaxel to cancer cells have been reported [76, 77]. This report detailed considerable improvements to several properties, such as sustained release, maximum tolerated dose [78] and increased bioavailability [79].

Along these same lines, we recently developed stealth polymeric nanoparticles stabilized by a non-immunogenic and non-toxic hydrophilic *N*-(2-hydroxypropyl)methacrylamide (PHPMA) copolymer. Stealth doxorubicin-loaded PBSBDL-PHPMA NPs that had pH-dependent doxorubicin (Dox) release were produced and *in vitro* cytostatic efficacy in EL4 T cell lymphoma was proven [80]. This approach enabled additional combination chemotherapy using simultaneous Dox and docetaxel (Dtxl) loading. Supramolecular assemblies comprising a Dtxl-loaded PBSBDL core and a Dox-conjugated HPMA-based copolymer shell were also produced. The use of nanoparticles simultaneously loaded with Dtxl and Dox more efficiently suppressed tumor cell growth in mice with EL-4 T cell lymphoma when compared with the effect of nanoparticles loaded either with Dtxl or Dox separately (discussed further in the section Summary of the Results – *vide* **publication 2**) [81].

Finally, the production of PLGA-based block copolymer micelles from PLGA-*b*-PEG and PLA-*b*-PEG has also been reported as a clever strategy to avoid rapid renal clearance of drug-loaded biodegradable polymeric nanoparticles. This category of nanomedicines is discussed in the next section.

2.2.3. Block copolymer nanoparticles

Polymeric micelles are generally produced in aqueous solution through the spontaneous self-assembly of amphiphilic block copolymers [82]. Amphiphilic block copolymers are polymers derived from two or more blocks of monomeric species with different chemical properties that are covalently bound. Upon water contact, the hydrophobic blocks tend to reduce their contact with the hydrophilic media leading to the formation of

generally spherical structures comprising a hydrophobic core stabilized by a hydrophilic shell. The size of block copolymer micelles is dependent on the polymer characteristics ranging usually from 10 to 100 nm [68, 83]. Therefore, lipophilic agents, such as hydrophobic drugs, can by solubilized in the micellar core, significantly affecting its concentration in aqueous media. The encapsulation efficiency is dependent on several parameters, including drug and polymer solubility parameters, size, shape and physical state of the hydrophobic guest molecule, as well as block copolymer length and volume ratio [44, 84]. Additionally, the active agents can also be attached to the hydrophobic segment of block copolymers *via* an environmentally responsive chemical bond. Therefore, controlled drug release can be achieved by triggering the chemical bond or by using polymers susceptible to environmental conditions, such as biological stimuli (pH-responsive, redox-responsive, enzyme-responsive polymers) or external stimuli (thermo-responsive, photo-responsive polymers) [44, 85-87].

Currently, most investigations are centered on biodegradable polymeric micelles because their degradability property circumvents micelle accumulation, which may lead to long-term toxicity. The employment of pH-responsive micelles is another clever approach because the polymers may be triggered and destabilized in response to the slightly acidic tumor microenvironment, enabling rapid release of active agents upon arrival at the desired site and simplifying renal clearance (further described in the section Summary of the Results – *vide* **publications 3-5**). One clever example is to devise block copolymers to produce nanoparticles comprising the PDPA (poly[2-(diisopropylamino)-ethyl methacrylate]) core (Figure 6). PDPA is a promising smart material for the construction of tumor-targeting drug delivery polymeric nanocarriers because it is able to encapsulate hydrophobic anticancer drugs and it undergoes a sharp hydrophobic-hydrophilic pH-induced transition within a pH range that is desirable for tumor-targeting drug delivery [88]. PDPA is one of the few polymers that can be loaded and that quickly release hydrophobic guest molecules at specific tumor sites *via* a pH-triggered pathway at slightly acidic conditions (further described in the section Summary of the Results – *vide* **publication 5**) [89, 90].

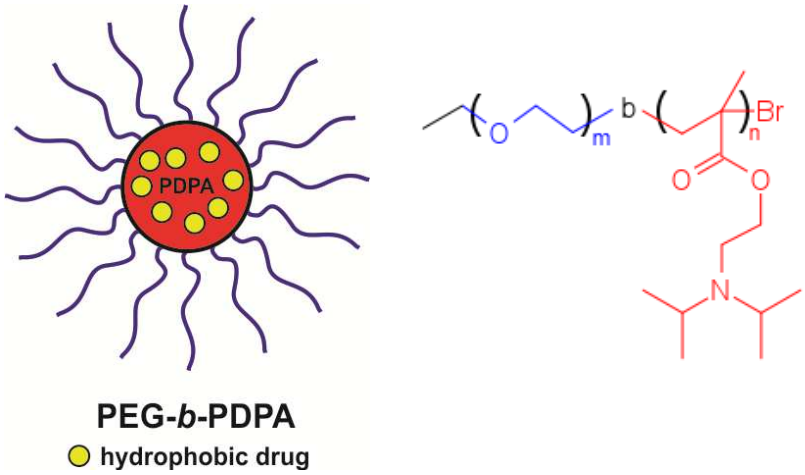

Figure 6. Schematic representation of a pH-responsive PEG-*b*-PDPA drug-loaded block copolymer micelle (*left*) and the molecular structure of the block copolymer PEG-*b*-PDPA (*right*).

Recent advances have been promoted by using other pH-responsive block copolymers. Supramolecular assemblies based on poly(lysine) and poly(histidine) may also have potential success because their pKa is approximately 6.0 - 7.0 [91, 92]. To our knowledge, there are no market products based on these special polymers; however, polymeric micelles based on poly(lysine) are already being examined in clinical trials.

2.2.4. Polymer-drug conjugates

The conjugation of drugs to synthetic and natural macromolecules (Figure 7) has been a long-term issue [49, 93-95]. The early conjugates reported were based on polyvinylpyrrolidone (PVP) conjugated to mescaline *via* a dipeptide (GL) spacer and based on poly(*N*-vinylpyrrolidone) conjugated to various antibiotics [94-95]. Nevertheless, only in the mid-seventies were polymer-drug conjugates envisaged as nanomedicines [49, 93, 96]. Ideally, polymer-drug conjugates should comprise a biocompatible polymer backbone as a vehicle and the active agent, which is bound to the polymer chain *via* a biologically responsive linker. Investigations into polymer-drug conjugates have become a fast and growing field with many conjugates being developed using a variety of responsive linkers. Undeniably, the optimization of polymer-drug linkers remains a main issue in the field. Polymer-drug linkers must be stable during bloodstream circulation and simultaneously should be able to release the conjugated drug at optimal rates upon arrival at the target site [93, 97]. The linkers are usually selected from the classes of cis-aconityl [98], hydrazone [99] (Figure 7), acetal [100], peptidyl [101], among other organic linkers [102].

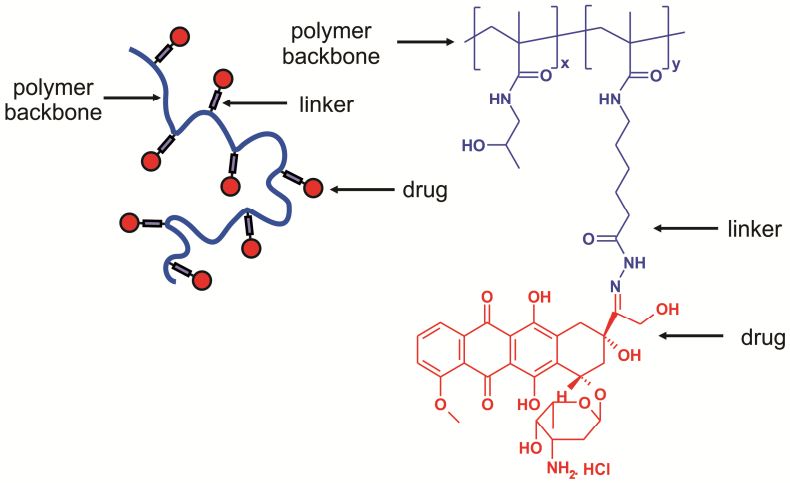

Figure 7. Schematic representation of a polymer-drug conjugate (left) and the molecular structure of the polymer-drug conjugate PHPMA-Dox, (right) where the active agent doxorubicin is covalently bound to poly[*N*-(2-Hydroxypropyl) methacrylamide] (PHPMA) *via* a pH-responsive hydrazone bond (R_1R_2C=NNH-).

Currently, the most intensely investigated polymer-drug conjugates are based upon highly hydrophilic polymers, such as PEG, PHPMA, poly(vinyl-pyrrolidone), poly(amino acids) and dextrans. The main advantages of these polymer-drug conjugates compared with the administration of the related free drug rely on the higher aqueous solubility of the attached hydrophobic drugs, the potential triggered release (pH, enzymes), enhanced drug bioavailability, prolonged plasma half-life, protection of the active agents against degradation and modified biodistribution (pharmacokinetics and pharmacodynamics). Linear, branched, star-like and multi-armed PEG-drug [103, 104] and HPMA-drug [95, 105, 106] conjugates have been previously investigated. Actually, linear PEG-drug conjugates are the simplest and most investigated systems. The active small molecules are usually conjugated to the distal end of the PEG chain. However, the primary limitation of this approach is the number of available conjugation sites. Consequently, branched and forked PEG-drug conjugates have been synthesized for the same purpose [103, 104, 107]. Similarly, multi-armed PEG has been widely investigated due to the presence of multi-hydroxyl or functional groups, increasing the number of available conjugation sites. Several multi-armed PEG-drug conjugates, such as NKTR-102 (PEG-irinotecan), EZN-2208 (PEG-SN38) and NKTR-105 (PEG-docetaxel), have entered into clinical trials for solid tumor treatment [103, 108].

PHPMA-drug conjugates are also frequently investigated. HPMA-Dox was the first synthetic polymer-drug conjugate to progress into clinical trials. The anticancer drug doxorubicin was attached to the HPMA copolymer *via* a biodegradable tetrapeptide spacer (GFLG). Clinical trials examining this polymer-drug conjugate initiated in the early 1990s [93, 96]. In the past few years, the selection of polymeric macromolecular

carriers, desired target (intracellular, endothelium, etc.) [109, 110], type of conjugation (direct or indirect) [97,111], linker chemistry [111, 112] and molecular weight [105] of PHPMA-drug conjugates has been extensively investigated to improve antitumor efficacy. Furthermore, the drug combination approach, where different agents are bound to the same macromolecular backbone has been successfully reported, *i.e.*, PHPMA-doxorubicin-aminoglutethimide [113], PHPMA-Dox-dexamethasone [114], PHPMA-Dox-gemcitabine [115], and PHPMA-Dox-Mitomycin C [116]. Subsequent investigations resulted in second-generation anticancer nanomedicines based on higher molecular weight HPMA-drug carriers containing enzymatically degradable bonds in the polymer backbone [94, 95]. The enhanced activity of the second-generation conjugates has been proven *in vivo* [106, 117].

Lastly, poly(amino acids)-drug conjugates based on poly(L-lysine) (PLL), poly(-aspartic acid) (PAA) and poly(L-glutamic acid) (PGA) have also been considered. PGA is the most accepted polymer in this class [118]. The pendant free γ-carboxyl group on each repeating unit of L-glutamic acid offers functional sites for drug attachment. Drug release is simplified because PGA itself biodegrades. PGA-paclitaxel (Opaxio^{TM}) and PGA-camptothecin have advanced to clinical trials.

2.3. Pre-clinical and clinical progress of soft matter based nanomedicines for cancer therapy

Considering clinical progress, although liposomes are the category with the highest number of marketed products and several more in clinical trials, there are a number of block copolymer micelles, polymer-drug conjugates and biodegradable polymeric nanoparticles currently in phase I/II, III and IV clinical trials to gain market approval. Some of these compounds have already received clinical status in specific countries. In this section will be highlighted the current status of the block copolymer micelles and biodegradable polymeric nanoparticles because they are the main goal of this thesis. The readers are invited to read the Appendix (*vide* **publication 1**) to gain more information related to the liposomes and polymer-drug conjugates designed for cancer chemotherapy, with regard to clinical trials as well as to formulations already in clinical use.

2.3.1. Biodegradable polymeric nanoparticles

Concerning biodegradable polymeric nanoparticles, doxorubicin loaded polyalkylcyanoacrylate (PIHCA) nanoparticles (Transdrug™/Livatag®) used to treat multidrug resistant hepatocarcinoma is one example that has progressed to clinical trials (currently in phase III) [119]. Transdrug™ allows doxorubicin to overcome multi-drug resistance (MDR) pumps [120], and its antitumour efficacy in patients with advanced hepatocellular carcinoma (HCC) has been confirmed [121]. In Phase II/III, Transdrug™ significantly increased survival rates in patients with advanced HCC (32 months compared with 15 months in patients receiving standard-of-care-treatment) [122]. Despite the significant 17 months difference, the clinical trial was interrupted due to frequent and severe pulmonary adverse events. Currently, the formulation is recruiting participants into Phase III clinical trials to determine whether Transdrug™ is effective treating patients suffering from advanced HCC after failure or intolerance to Sorafenib [123].

Correspondingly, promising results have been demonstrated for HCC treatment using mitoxantrone (dihydroxyanthracenedione, DHAD) loaded into polybutylcyanoacrylate (DHAD-PBCA) nanoparticles (47% of DHAD) [124]. The activity and toxicity of these NPs against HCC were evaluated in a randomized multicenter Phase II study [125]. The DHAD-PBCA NPs increased cytotoxicity in hepatic tumors and extended the mean survival time from 3.23 months (patients receiving free DHAD) to 5.46 months.

2.3.2. Block copolymer nanoparticles

There are several drug-loaded polymeric micelles currently in Phase I/II, III and IV clinical trials, specifically for the delivery of Dox and PTX [126, 127]. To the best of our knowledge, Genexol®-PM, a PTX formulation based on monomethoxy-PEG-*b*-poly(D,L-lactide) (MPEG-PDLLA), is the only formulation approved in this category (South Korea, Bulgaria and Hungary) for the treatment of cancer (breast, lung and ovarian cancer). The Genexol®-PM efficacy has been demonstrated in a Phase II clinical trial in patients with breast cancer [128] and in patients with advanced non-small cell lung cancer (NSCLC) when combined with cisplatin [129]. Peripheral neuropathy and myalgia adverse events were observed. However, acute hypersensitivity reactions, which are common during Taxol® and Taxotere® treatment, were not observed [128].

Genexol®-PM is currently undergoing Phase IV clinical trials [130] and therapies combined with other antitumor drugs are being developed [131].

Regarding poly(amino acids)-based block copolymer micelles, NK105 is a PTX-loaded micellar system prepared from PEG-poly(aspartic acid, Pas) (PEG-*b*-Pas), where PTX is physically entrapped (~ 23% $w_{drug}/w_{polymer}$). The nanocarrier-based formulation underwent a Phase II clinical trial against advanced or recurrent gastric cancer in 2010, demonstrating modest activity and tolerability [132]. Phase III studies in patients with breast cancer are being designed to elucidate its survival benefits [133]. Cisplatin incorporation into PEG-*b*-PGlu micelles resulted in the NC-6004 formulation. The cisplatin was incorporated *via* polymer-metal complex-formation [134]. During Phase I clinical trials in patients with solid tumors it reduced toxicity and stabilized the disease (7/17 patients) [135]. A Phase I/II clinical trial of NC-6004 combined with gemcitabine for metastatic pancreatic cancer treatment was conducted in Asia; the results demonstrated the good tolerability and acceptable efficacy of the combination [127]. Phase III studies of NC-6004 in combination with gemcitabine to determine their efficacy *versus* gemcitabine alone in patients with advanced or metastatic pancreatic cancer are currently being designed [136].

Similarly, in the formulation NK012 the agent 7-ethyl-10-hydroxy-camptothecin is chemically conjugated to the PGlu segment of PEG-*b*-PGlu, and the self-assembly resulted in 20 nm sized drug-loaded block copolymer micelles. This formulation demonstrated promising antitumor activity in Phase I clinical trials in patients with advanced solid tumors [137]. The safety and efficacy of NK012 for advanced and metastatic triple negative breast cancer treatment is ongoing (Phase II) [138], as well as, for colorectal cancer treatment in combination with 5-fluorouracil (Phase I) [139]. Similarly, NK911 is a micellar nanocarrier (~ 40 nm) consisting of a PEG-poly(aspartic acid) block copolymer conjugated to doxorubicin. Phase I investigations demonstrated a partial response (1/23 patients) or stable disease (8/23) in patients with metastatic pancreatic cancer [140]. However, its plasma clearance was ~ 400-fold higher compared with Doxil® suggesting that the NK911 has lower stability in the bloodstream. The formulation NC6300 consists of epirubicin covalently bound to PEG-*b*-polyaspartate block copolymers *via* an acid-labile hydrazone bond. This conjugate produces 40-80 nm micellar structures and is intended to be indicated for breast cancer. In pre-clinical studies, prolonged blood circulation with preferential accumulation in human liver and breast cancer xenograft models was reported [141], along with extended antitumor effects with reduced epirubicin cardiotoxicity in mice bearing Hep3B liver orthotopic tumors [142]. Following preclinical evaluations, a Phase I trial is underway in Japan in patients with advanced or metastatic solid tumors [143].

The micellar doxorubicin formulation SP1049C has been produced from the well-known class of Pluronic® micelles. This nanocarrier has demonstrated higher antitumor effects compared with the free parent drug [144, 145]. SP1049C safety and efficacy was demonstrated in Phase II investigations in patients with advanced adenocarcinoma of the esophagus and gastroesophageal junction (9/19 patients had a partial response and 8/19 patients had either a minor response or stable disease) [146].

The aptamer-conjugated PLGA-PEG-docetaxel nanoparticle (BIND-014) is an example of a ligand-mediated targeting nanocarrier able to recognize PSMA (prostate-specific membrane antigen) expressed on the cancer cell surface. This formulation was well tolerated with predictable and manageable toxicities in Phase I clinical trials [30]. These promising results are currently being continued in a Phase II trial in patients with advanced or metastatic solid cancers [147] or with metastatic castration-resistant prostate cancer [148].

2.4. Main challenges to move forward

Although the convergence of fundamental and applied research has contributed to the development of novel nanotechnology-based medical technologies that are commercially marketed products, numerous soft matter-based formulations have disappointed in clinical trials. This highlights the necessity of careful optimization and control over polymer chemistry and supramolecular assemblies to improve the stability and efficacy of cancer therapies. Furthermore, in addition to the vehicle-related challenges, the specific features of each tumor and each patient appears to be the most difficult barrier to further progress. The current primary developmental challenges are summarized in this section as vehicle-related and physiological-related barriers.

2.4.1. Vehicle-related barriers

The practical challenges related specifically to polymeric micelles depend on poor *in vivo* stability due to extensive dilution upon injection, resulting in vehicle dissociation [140, 149]. To date, approaches to overcome this issue are based on crosslinking strategies [150]. Another issue is inefficient cellular uptake of polymeric micelles by the target cancer cells. This is caused by the presence of dense layers of stealth polymers, such as PEG, in the outer shell of the assemblies, which is required to promote long circulation of the entities in the bloodstream [151]. To achieve high drug accumulation using stealth nanocarriers, one clever strategy is the use of pH-responsive polymers that promote pH dependent dissociation of the nanocarriers upon arrival at the

tumor site. This phenomenon occurs in response to the slightly acidic tumor microenvironment compared with physiological pH. Small molecular weight anticancer drugs are then able to be internalized by a simple diffusion process rather than endocytosis. Regarding polymer-drug conjugates, polymer-drug linker optimization to ensure stability during circulation is extremely important because rapid hydrolysis and drug elimination may explain many of the disappointing results obtained during clinical trials. Furthermore, high drug-loading (physically entrapped or covalently bounded) is also required. Considering the class of liposomes, drug leakage and stability during bloodstream circulation limits the higher efficacy. However, cholesterol incorporation into the bilayer, thereby increasing cohesiveness and reducing leakage, has been employed to circumvent these difficulties [152, 153].

Generally, structural parameters, such as size, shape and surface charge, have been shown to influence cellular uptake. The tumor pore size depends on tumor permeability, type, heterogeneity and tumor progression [11]. The tumor pore size usually ranges from ~ 10 nm to 2 μm [11, 15, 18, 19]. However, nanoparticles ranging from 10 nm to 200 nm have been shown to be preferentially accumulated *via* the EPR effect [20]. Liposomes accumulate more when their dimensions are approximately 100 nm [154], whereas only micelles ~ 30 nm can penetrate into hypovascular tumors [155]. As a "rule of thumb" , polymer-drug conjugates should have molar mass below ~40 kDa and be small enough to be renally filtered [156]. Regarding surface charge (zeta potential), opsonins tend to bind to charged or hydrophobic polymers accelerating hepatic clearance [157, 158]. The effect of soft colloid surface charge and its influence on body clearance remains controversial [159-163]. The shape of nanomedicines significantly impacts pharmacokinetics and tumor accumulation. Water soluble polymers are usually flexible and are therefore able to deform to easily pass through pores, whereas rigid structures, such as star-like and hyperbranched polymers, may encounter more difficulty [156]. For example, filomicelles persist in circulation ten times longer than their spherical counterparts [164]. The *in vitro* cell internalization of differently shaped cationic cross-linked PEG hydrogels demonstrates that the internalization of rod-like structures occurs more rapidly and efficiently compared with other shapes with the same volume and size [159].

Therefore, considering the above-mentioned issues, the precise control and optimization of these parameters will lead to improved nanomedicine design for use in various biomedical applications. To this end, the Table 1 summarizes the main advantages and the drawbacks of the above-mentioned soft matter based nanomedicines.

Table 1. Advantages and drawbacks of different soft matter based nanomedicines.

System	Main advantage	Main drawback
Liposomes	encapsulation of hydrophilic and/or hydrophobic agents both drugs formulated in non-covalent way biodegradability	usually large structures which may reduce extravasation efficiency drug leakage (instability of system during storage and transport to target tissue) no simple manufacturing
Biodegradable polymeric nanoparticles	simple manufacturing size control stability during circulation biodegradability agents can be formulated in a non-covalent way	surfactants for stabilization physically incorporation of just hydrophobic agents
Block copolymer micelles	small size enabling effective EPR accumulation agents can be formulated in a non-covalent way biodegradability simple manufacturing	Poor in vivo stability and possible dissociation upon injection limited loading capacity physically incorporation of just hydrophobic agents
Polymer-drug conjugates	higher aqueous solubility of attached hydrophobic agents high loading capacity stability during circulation encapsulation of hydrophilic and/or hydrophobic agents	instability of polymer-drug linkers no simple manufacturing non biodegradability agents must have suitable functional groups

2.4.2. Physiological-related Barriers

In addition to vehicle-related issues, tumor concerns must also be addressed to realize the desired expectations of nanomedicines in cancer chemotherapy. Physiological barriers are undoubtedly the most important limiting factor against enhancing the efficacy of nanotechnology-based therapies. Firstly, blood vessel fenestrations in tumor sites vary substantially. However, the pore size of brain tumor tissues usually does not exceed 10-12 nm [15]. This particular feature challenges nanoparticle design for brain tumor treatment because the assemblies are rapidly cleared *via* renal filtration when the sizes are less than 10 nm [165, 166]. Tumor pore

size is dependent on physiological conditions, which vary substantially from tumor to tumor and from patient to patient [11, 25, 26, 30]. Furthermore, differences in tumor treatments have been observed in pre-clinical models (animals) to further clinical trials (humans). This is thought to be related to tumor-related physiological differences between species and studies, *i.e.*, tumor biology and clearance differ between animals and humans and pre-clinical models usually are focused on primary tumors, whereas clinical trials are conducted in metastatic patients [30]. Although there has been significant progress controlling the physical parameters of nanomaterials, this issue restricts the optimization of colloidal system requirements because differences in tumor treatments and tumor models hinder efficient accumulation. Ideally, this issue will be resolved by the personal design of nanomaterials.

Additionally, as nanomaterials reach tumor sites, passively or actively, permeation efficacy depends on tumor type, status and location [11, 20, 21, 30]. Another major challenge is the tumor negative pressure gradient because the interstitial pressure is higher in the tumor core, and therefore, the nanoparticles will always have the tendency to flow towards the periphery. A clever strategy for this issue is to increase blood pressure, reducing the pressure difference and ideally improving passive nanomaterial accumulation [167]. Furthermore, the EPR effect itself is highly heterogeneous and usually accumulation is not even, particularly in the central regions of the malignancy.

Finally, tumor resistance and MDR resistance are issues that must be considered. The strategy to circumvent these factors may lie in the field of ligand-mediated active targeting through the development of systems to target the endothelium of the tumor vasculature [25, 48] because endothelial cells have higher circulation accessibility and the tissue is genetically stable limiting the development of tumor resistance [168]. Combined therapy may be a promising strategy to suppress cancer-drug resistance because different drugs may damage or kill cancer cells during different stages of their growth cycles [105]. The co-delivery of multiple drugs through a single administration has advantages, such as possible synergistic therapeutic effects, suppression of drug resistance and the ability to control drug exposure [105, 137, 139].

2.5. Non-responsive soft matter assembles for cancer chemotherapy

2.5.1. Non-responsive biodegradable polymeric nanoparticles based on human metabolism monomers as drug-delivery systems

The use of biodegradable and biocompatible polymers to prepare systems as potential biomaterials has become one important area of materials in medicine. Due the advances in polymer chemistry and polymer colloids, it is nowadays possible to prepare polymers exhibiting unique finely tuned properties which are required to achieve the goal of biomedical applications [169-171]. Biodegradable polymers are very attractive because through the optimization of the degradation it is possible to allow the body clearance of the polymeric material avoiding its accumulation and possible toxicity [172, 173]. Nevertheless, the available biodegradable polymers suitable for biomedical applications are limited due to the essential requirement of biocompatibility. Furthermore, the degradation mechanism must also not lead to the formation of toxic products [174].

However, over the past decades, the use of biodegradable polymers aiming at the preparation of nanoscale and biomedical devices has been mostly limited to the aliphatic polyesters such as PCL, PLA and PLGA essentially due to their good hydrolyzability, biocompatibility and degradation properties [175, 176]. Heretofore, the selection of the biocompatible monomer to be used as future biodegradable polymer candidate is a subject of fundamental relevance in biomedical applications. The use of metabolite monomers that are normally present in the human metabolism offers a route to minimize toxic side effects. Some of these polymers, during degradation, release molecules that the body can resorb, metabolizing them in various physiological pathways [172].

Some examples of monomers endogenous to the human metabolism are succinic acid (SA) and saturated dilinoleic acid (DLA). Succinic acid is a key intermediate in the Krebs cycle (also known as the citric acid cycle) [177]. DLA is a fatty acid derived from the dimerized linoleic acid. Numerous physiological benefits have been attributed to linoleic acid derivatives including action as an anticarcinogenic [178, 179], antiatherosclerotic [180] and antidiabetogenic agent [181]. Moreover, fatty acids are suitable components to the preparation of biodegradable polymers since they are hydrophobic naturally occurring body compounds [182]. Different fatty acid monomers obtained from natural sources have been suggested as starting materials to produce devices for biomedical applications resulting in copolymers of numerous structures [183].

Recently, multiblock copolymers composed by SA, 1,4 butanediol (BD) and dilinoleic acid as building block monomers were proposed as a suitable biomaterial for bone and tissue engineering demonstrating good biocompatibility [183, 184]. DLA is the dimerized linoleic acid and it is a suitable monomer for step growth polycondensation resulting in copolymers of numerous structures [185, 186, 187, 188]. Hence, DLA copolymer-based biodegradable and biocompatible polyesters can render very interesting biomaterials usable as nanocarriers, they deserve to be investigated for such a purpose. Although copolymers containing fatty-acids monomers as building blocks were extensively proposed in the literature as devices in many biomedical applications, the application of DLA as building blocks for copolyester synthesis aiming at drug delivery purposes through polymer nanoparticles were just reported recently. [69] Surfactant-free sub-100 nm in diameter biodegradable and biocompatible nanoparticles was prepared by the well-known nanoprecipitation approach. Their characterization and preliminary evaluation of the biological behaviour was also described [69, 80] as well as the co-delivery of multiple anticancer drugs to solid tumors providing more efficient suppression of tumor-cell growth and increase of animal survivor in mice [81].

Taking into account the benefits of SA, BD and DLA as building block monomers from the human metabolism, a new series of renewable resource-based biodegradable and biocompatible copolyesters was synthesized by environmentally benign melt polycondensation. The polymers and the nanoscale delivery systems prepared from them were further characterized in detail employing several standard techniques. Their capabilities to prepare biodegradable and biocompatible non-responsive soft polymer nanoparticles for chemotherapeutic delivery is deeply detailed and discussed throughout the section Summary of the Results (*vide* **publication 2**).

2.6. Responsive polymer nanoparticles for cancer chemotherapy

For potential drug delivery applications, ideal drug carriers need to combine both the targeting property and the stimulus responsiveness to enhance the bioavailability of the drug as well as to reduce the side effect.[189] Therefore, designing stimulus-responsive nanoparticles for programmed drug delivery, which release the drug in a controlled manner on arrival at the targeted site, is highly desired. Stimulus-responsive nanoparticles produce physical or chemical changes when subjected to external signals, including variations of macromolecular structures, solubility, surface properties, swelling and dissociation. The examples and classification of biological stimuli that can be exploited for triggering the delivery of drugs, genes, or diagnostic

agents from the nanocarriers are diverse and manifold in nature. Though overlapping in many instances, the stimuli that trigger drug release from the nanocarriers can be broadly classified with respect to the biological systems as either internal (physiological, pathological, and patho-chemical conditions) or external (physical stimuli, *e.g.*, heat, light, magnetic and electrical fields) (Figure 8) [190-193].

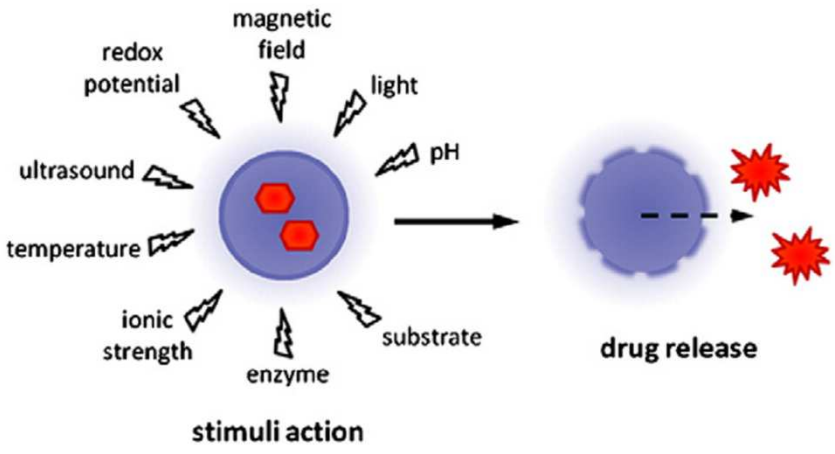

Figure 8. General scheme of stimuli-responsive release of a drug from a nanocarrier [193].

Along the thesis two specific internal stimuli (physiological/pathological) will be exploited as a target to drug release, the stimuli to differences in pH and in to the production of reactive-oxygen-species (ROS). Both of them are detailed below.

2.6.1. Responsive polymer NPs to pH-cellular imbalances

The choice of using pH-sensitivity is mainly due to the presence of a sharp pH gradient across biological systems on both cellular and systemic levels in pathological states which differ from the physiological pH of 7.4. For many years, the shift of pH status in the gastro-intestinal systems from very acidic to basic (~2.0 – 8.0) has been taken into consideration in the design of orally-active pH-sensitive prodrugs and controlled release delivery systems [194]. In cellular and sub-cellular levels, the pH factor plays an even higher and more critical role since abnormal tissue, as in inflamed, infected, or malignant tissue usually demonstrates lower pH values. In cancer tissues the extracellular pH can easily fall to values around 6 - 7 while for certain cancers it reaches even lower values. [195] After cellular uptake *via* endocytosis, the nanocarrier system faces very well-defined

compartments with strongly differential pH status. The early endosome has a pH about 5 - 6 while the late lysosome, which is the most acidic compartment, has a pH around 4 – 5 [196] (*vide* section **Intracellular Delivery of Active Agents**). These extra- and intracellular pH gradients will be used herein to design drug delivery systems which selectively release their transported drug at the specific site of action.

2.6.2. Responsive polymer NPs to reactive oxigen species (ROS) cellular imbalances

In the human body, there are two types of oxidative species: reactive oxygen species (ROS) and reactive nitrogen species (RNS). ROS generally include the superoxide anion and hydrogen peroxide (H_2O_2), which are initially generated by oxygen reduction, as well as, their derived reactive species including the hydroxyl radical, hypochlorous acid (HOCl), peroxyl radicals, and singlet oxygen. Herein, ROS it will be exploited as a target for programed drug delivery.

ROS have a crucial role in human physiological and pathophysiological processes. An emerging body of data indicates that ROS such as H_2O_2 act as a component of cell signaling pathways that is necessary for the growth, development, and fitness of living organisms. However, imbalances in H_2O_2 production lead to oxidative stress and inflammation events, which damage tissue and organ systems and are correlated with the onset and advancement of various diseases, including cancer, diabetes, cardiovascular and neurodegenerative diseases. The involvement of ROS in cellular signaling and disease states has motivated the construction of chemical tools to ROS-specific detection systems, and ROS-responsive micro- or nanocarriers. [197-201] Delivery platforms that enable targeted release of antioxidants or chemotherapeutic drugs at sites of high ROS activity have the potential for high therapeutic impact. The ability to generate a triggered nanoparticle response (*e.g.*, release of cargo or polymer degradation) in the presence of ROS rich microenvironments is of particular interest, *e.g.*, in targeted delivery to tumors and sites of inflammation. Such delivery is achieved since the aforementioned tissues exhibit enhanced accumulation and uptake of macromolecules and nanoparticles (with diameter less than 100 nm) through the combination of their generally leaky microvasculature and missing or tight lymphatic capillary systems. This effect is the already mentioned EPR effect, known also for solid tumors. Furthermore, both microenvironments share lower pH values if compared to the pH of normal tissues. These biological features inspired us to exploit the imbalances in the ROS cellular levels on the healthy and unhealthy microenvironments to develop systems for the *in vitro* (*in vivo*) detection of different ROS or the *in vivo* diagnosis of oxidative stress-relevant diseases, *e.g.*, cancer, diabetes, cardiovascular and neurodegenerative

diseases. The most utilized ROS momoners are depicted in the Figure 9. The phenylboronic acid based systems are the most promising and ROS-sensitive reported up-to-date [202, 203].

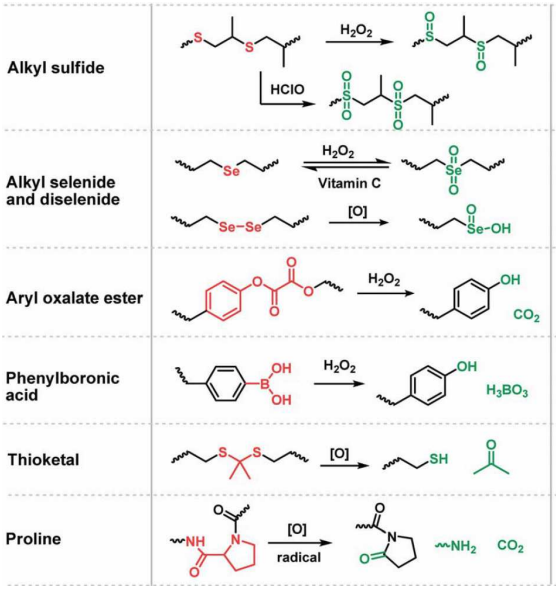

Figure 9. Oxidation-responsive motifs and their oxidation products. [Modified from ref. 203]

Taking into account the aforementioned, the thesis was driven to the preparation of NPs based on the promising soft matter assemblies that have entered in clinical trials, *e.g.*, the biodegradable polymeric NPs and the block copolymer NPs. The systems were prepared taking advantages based on the vehicle-related barriers and physiological-related barriers (*vide* section **2.4.1** and **2.4.2**) and are described in the following sections as **publications 2** to **6**.

3. List of publications included in the thesis

Publication 1
Jäger, E and Giacomelli, F.C.: Soft matter assemblies as nanomedicine platforms for cancer chemotherapy: a journey from market products towards novel approaches.
Current Topics in Medical Chemistry **2015**, *15,* 328-344.

Publication 2
Jäger, E., Jäger, A., Chytil, P., Etrych, T., Říhova, B., Giacomelli, F.C., Štěpánek, P., Ulbrich, K. Combination chemotherapy using core-shell nanoparticles through the self-assembly of HPMA-based copolymers and degradable polyester.
Journal of Controlled Release **2013**, *165,* 153-161.

Publication 3
Petrova, S., **Jäger, E.**, Konefał, R., Jäger, A., Venturini, C.G., Spěváček, J., Pavlova, E., Štěpánek, P. Novel poly(ethylene oxide monomethyl ether)-*b*-poly(ε-caprolactone) diblock copolymers containing a pH-acid labile ketal group as a block linkage.
Polymer Chemistry **2015**, *5,* 3884-3893.

Publication 4
Jäger, E., Jäger, A., Höcherl, A., Petrova, S., Venturini, C.G., Janouškova, O., Konefał, R., Ulbrich, K., Pavlova, E., Štěpánek, P. pH-triggered cargo release through nanoparticles based on biodegradable block copolymer containing a ketal groups as a block linker.
RSC Advances Communication **2015**, manuscript under review.

Publication 5
Jäger, A., **Jäger, E.**, Surman, F., Angelov, B., Ulbrich, K., Drechsler, M., Garamus V., Rodríguez Emmenegger, C., Nallet, F., Štěpánek, P. Nanoparticles of poly([*N*-(2-hydroxypropyl)]methacrylamide)-*b*-poly[2-diisopropylamino)ethyl methacrylate] diblock copolymer for pH-triggered release of paclitaxel.
Polymer Chemistry **2015**, *6,* 4946-4954.

Publication 6
Jäger, E., Höcherl, A., Jäger, A., Štěpánek, P., Hrubý, M., Konefał, R., Netopilik, M., Pánek, J., Šlouf, M., Ulbrich, K. Fluorescent boronate-based polymer nanoparticles with reactive oxygen species (ROS)-triggered cargo release for drug-delivery applications.
Nanoscale **2015**, manuscript under review.

4. Summary of the results

4.1 Soft matter assemblies as nanomedicine platforms

This section summarizes the approaches and results included in **publications 1** to **6**. According to the aims of the thesis, these results are divided into four main research topics. The first topic is a summary of the current medical applications of nanotechnology and the potential of the emerging field of nanomedicine embraced as introduction of the present thesis. It was focused in the recent advances in the manufacture of soft matter-based nanomedicines specifically designed to improve diagnostics and cancer chemotherapy efficacy. It has particularly highlighted liposomes, polymer-drug conjugates, drug-loaded block copolymer micelles and biodegradable polymeric nanoparticles, depicted in Figure 10, emphasizing the current investigations and potential novel approaches towards overcoming the remaining challenges in the field, as well as, formulations that are in clinical trials and marketed products. These topics are fully detailed in the **publication 1** (*see* Appendix) as a review.

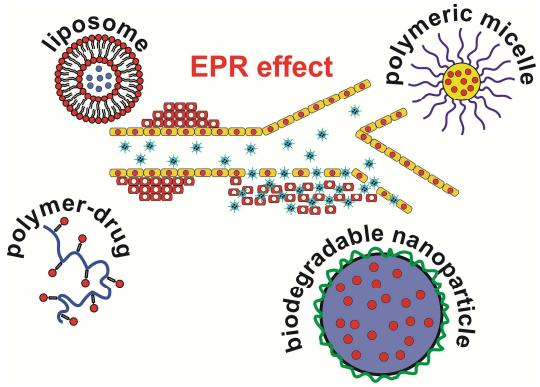

Figure 10. Main classes of soft matter nanomedicines in cancer therapy.

4.2 Combination chemotherapy trough non-responsive soft matter assemblies as nanomedicine platforms (*publication 2*)

A novel approach for nanoparticle-based combination chemotherapy simultaneously incorporating two different antitumoral agents into a single polymeric nanoparticle is herein briefly discussed and fully reported in the **publication 2** (*see* Appendix). The self-assembly of a new aliphatic biodegradable copolyester PBSBDL (poly(butylene succinate-*co*-butylene dilinoleate)) and a HPMA-based copolymer containing cholesterol

(PHPMA-chol) (Figure 11) units enables preparation of narrowly distributed sub-200 nm "stealth" degradable polymeric nanoparticles, which are suitable for passive tumour targeting and combination chemotherapy *in vivo*.

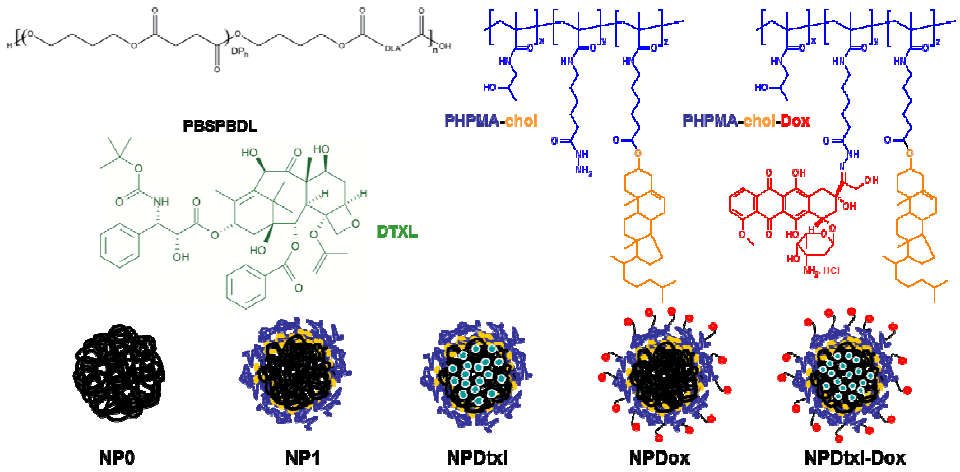

Figure 11. Molecular structure of the PBSBDL copolyester - left, PHPMA-Chol - middle and PHPMA-chol-Dox - right **(**top**)** and schematic representation of the produced NPs **(**bottom**)** (PBSBDL - black, PHPMA - blue, cholesterol anchor - yellow, Dtxl - green, Dox - red).

Recently, it has been shown that in comparison to well-known standard polyesters such as PCL, PLGA and PLA, the PBSBDL as spherical surfactant-free NPs can cargo a higher paclitaxel amount (~ 6 - 7 % $w_{drug}/w_{polymer}$). The NPs were shown to be highly swollen by water and bulk erodible in about two weeks due to their porous structure [69], which accelerates the hydrolysis process, being very attractive characteristic aiming at drug delivery applications. Therefore, the PBSBDL copolyester was selected as the biodegradable core forming of the nanoparticles. As a "stealth" shell forming polymer the precursor PHPMA-Chol was prepared by free radical terpolymerization of HPMA with comonomers bearing hydrazide groups and the cholesterol hydrophobic substituents. The macromolecular characteristics of the polymers are given in Table 2 and the synthetic procedures are fully described in the **publication 2** (*see* Appendix).

The PBSBDL copolyester and the PHPMA-based polymers were synthesized with M_w below the renal threshold (M_w ~ 50 kDa) allowing the polymer to undergo renal clearance avoiding accumulation after *in vivo* administration [204].

Table 2. Macromolecular characteristics of the synthesized polymers.

Entry	M_n (10^3 g·mol^{-1})[a]	M_w / M_n[a]	Cholesterol amount (mol%)[b]	DOX (*w*t.%)[c]
PBSBDL	32.0	1.76	-	-
PHPMA-Chol	17.2	1.92	2.3	-
PHPMA-Chol-Dox	21.1	1.65	2.3	10.1

[a] Measured by SEC; [b] Determined by ^{1}H NMR; [c] Measured by UV/Vis spectrophotometry.

The structure of the nanoparticles was characterized in detailed by SLS, DLS and ELS (Table 3 and Appendix) besides TEM (Figure 12). The size of the core-shell NPs (R_H) was found to be always below the cut-off size of the leaky pathological vasculature ($2R_H$ < 200 nm) thus making them potential candidates for the use in targeted cancer chemotherapy *via* passive solid tumour targeting due to EPR effect.

Table 3. Physicochemical characteristics of the produced NPs.

Entry	R_H (nm)	Dispersity[a]	ζ (mV)	$M_{w(NP)}$ (10^7 g·mol^{-1})	R_G (nm)	d (g·mL^{-1})
NP0	46.0	0.10	-32.0	12.9	47.0	0.46
NP1	41.0	0.09	-26.0	4.2	38.0	0.24
NPDTXL-Dox*	56.0	0.09	+17.0	23.3	61.0	0.53
NPDox	54.0	0.08	+15.0	21.7	59.0	0.55
NPDtxl**	44.0	0.06	-21.0	6.4	40.0	0.30

[a]estimated using the Cumulants analysis of the autocorrelations functions monitored at 90°. * NPs loaded with docetaxel (Dtxl) and doxorubicin (Dox). ** NPs loaded just with docetaxel (Dtxl).

The formation of spherical core-shell nanoparticles was confirmed by TEM. The Figure 12 reveals that the NPs are constituted of an electron-dense compact core and a thicker shell which is highly diffuse.

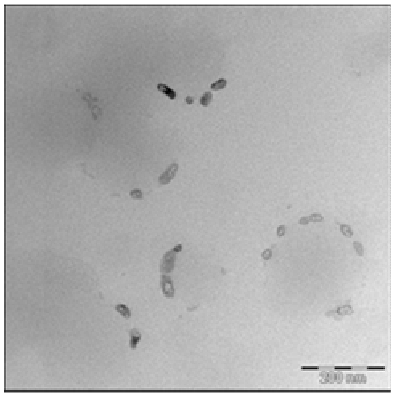

Figure 12. TEM image of NPDtxl-Dox.

The efficient NPs accumulation into solid tumour sites requires long circulating capability to enable time-dependent extravasation of the NPs through the leaky blood tumour microvasculature. The long-time stability of NPs in serum is therefore a pre-requisite for the use of polymeric NPs *in vivo* [80, 155]. In order to confirm the serum stability of the NPDtxl-Dox NPs they were incubated in 10% (*v*/*v*) diluted human plasma in PBS. The serum stability of the NPs was monitored by evaluating possible changes in hydrodynamic size and scattering intensity over time [88]. The temporal stability of the NPs in blood plasma as a function of the incubation time is given in the Appendix (*vide* **publication 2**, Fig. 6). The size and scattering intensity patterns of the nanocarrier system does not change within the first 24 h suggesting that the NPs are highly stable against aggregation in the simulated physiological media. The slight increase in hydrodynamic radius ($2R_H$ ~ 122 nm; size increase in ~ 10 nm) is supposed to be related to the adsorption of a protein monolayer since the average size of the dissolved single proteins is ~ 8 nm [205].

The stability of the NPs is promoted by the presence of the hydrophilic PHPMA shell since the HPMA copolymers exhibit hydrophilicity making energetically unfavourable the adsorption of plasma proteins. The serum stability points out that the PHPMA coating was efficient to provide "stealth" property to the manufactured nanomedicines. The novel nanoparticle carrier-based nanomedicines designed for targeted drug delivery take advantage of the combination of activity of highly hydrophobic drug docetaxel (Dtxl) entrapped physically within the degradable polyester core and the hydrophilic drug doxorubicin hydrochloride (Dox.HCl) conjugated to the reactive HPMA copolymer shell *via* hydrazone bond enabling its pH-sensitive release. The release experiments were conducted at 37 $^{\circ}$C and pH 7.4 (to simulate conditions during transport in blood) and at pH 5.0 (buffer modelling acidic cytosolic or endosome conditions in tumour cells). The profiles are given in Figure 13. The Dtxl sustained release was observed where 39 % and 31 % of the loaded Dtxl was released within

the first 12 h of incubation at pH 7.4 and pH 5.0, respectively. The remaining Dtxl was slowly released where only 56% and 49% was released at pH 7.4 and pH 5.0 within 48 h of incubation. The slow Dtxl pharmacokinetics is attributed to the hydrophobicity of the manufactured PBSBDL core and to the poor water solubility (~ 0.025 $mg{\cdot}mL^{-1}$) of Dtxl. In the current case, the drug release is also supposed to be controlled by the diffusion of the drug through the polymer matrix and by the hydrolysis of the biodegradable PBSBDL copolymer. On the other hand, a reasonable small amount of Dox (10%) was released in the same period at pH 7.4 whereas more than 87% was released within the same period at the pH mimicking the intracellular environment (pH 5.0). The release data demonstrates that during the systemic circulation only marginal amounts of drugs is released before reaching solid tumour environments *via* the EPR effect mechanism. Conversely, the Dox is quickly released at pH 5.0 where ~ 42 % of the loaded Dox is released within first 12 h whereas the anticancer drug is almost integrally released within 48 h fulfilling the criteria for pH-triggered drug release mechanism. Therefore, the core-shell NPDtxl-Dox exhibit physicochemical properties required for practical application as nanocarriers in passive tumour-targeted drug-delivery. The fastest Dox release profile at pH 5.0 and the slow Dtxl release kinetic is a strong hint that the co-delivery system can provide synergistic effect in the treatment of solid tumors.

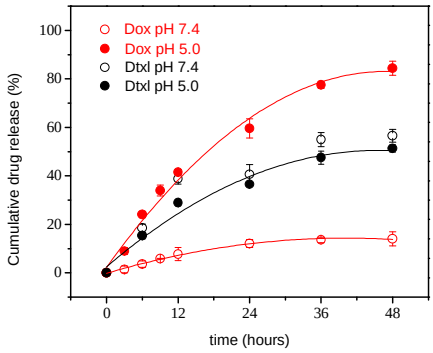

Figure 13. Dtxl and Dox release profiles from core-shell NPDtxl-Dox at pH 5.0 (Dtxl ●; Dox ●) and pH 7.4 (Dtxl ○; Dox ○). The values represent average ± s.d. (n = 3).

The use of nanoparticles simultaneously loaded with Dtxl and Dox.HCl provided a more efficient suppression of tumor cells growth in mice bearing EL-4 T cell lymphoma when compared to the effect of nanoparticles loaded either with Dtxl or Dox separately. Additionally, the obtained self-assembly nanoparticle platform enables further development of targeting strategies based on the use of multiple ligands attached on a shell surface for simultaneous passive and active targeting and combination therapies.

The anticancer activity of the produced NPs was evaluated in mouse syngeneic lymphoma model. The developed tumours killed the untreated mice within 28-32 days (the mean survival time was 30 days, SD=1.87, median survival 28.5 days, n=8). The NPs were administered in two doses (2×5 mg Dox(equivalent)/kg) on the 7th and 8th day after tumour transplantation. The treatment of mice inoculated with EL4 T cell lymphoma by using NPDtxl-Dox was substantially more effective than the treatment with free drugs or with single-loaded NPs (NPDtxl or NPDox) as reported in Figure 14. After 30 days of treatment using NPDtxl or NPDox, the tumour growth was reduced by ~ 50% and ~ 65% respectively, as compared to the controls ($p < 0.005$). The NPDtxl-Dox NPs inhibited the tumour growth by ~ 90% compared to the controls (30 days, $p < 0.001$) or by ~ 30% compared to NPDtxl and NPDox NPs ($p < 0.005$). It is worthwhile to highlight that the co-delivery also suppressed tumour growth more efficient than the delivery of either free Dox or free Dtxl at the same dose concentrations. Along with the reduction of tumour growth, the survival time of the animals under cancer chemotherapy was also extended compared to the untreated controls (Fig. 14b). The efficacy of the combination chemotherapy (NPDtxl-Dox) in comparison to NPDtxl and NPDox (dose-equivalent) is evident. Mice treated with core-shell NPDtxl-Dox survived significantly longer compared with untreated control of separately administrated Dox and Dtxl. This might indicate a synergistic effect to be further investigated.

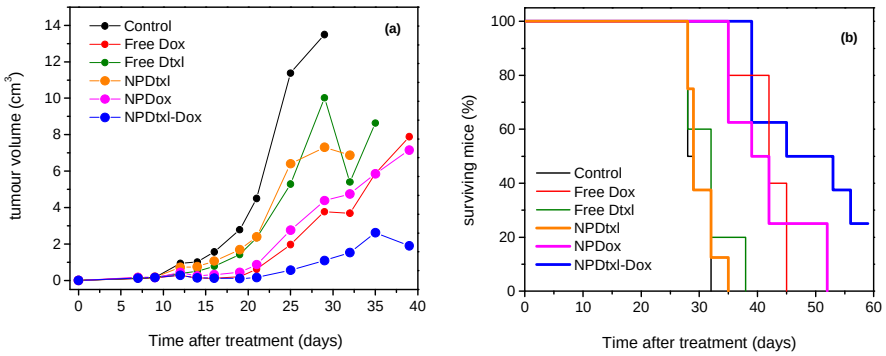

Figure 14. *In vivo* effect of core-shell NPs on the growth of T cell lymphoma EL-4 (a), Kaplan-Meier survival plot of mice (b); NPDtxl (-) 2 × 5 mg Dox(equivalent)/kg, NPDox (-) and NPDtxl-Dox (-) 2 × 5 mg Dox(equivalent)/kg, Free Dtxl (-) 2 × 5 mg Dox(equivalent)/kg; Free Dox (-) 2 × 5 mg Dox(equivalent)/kg, untreated control (-) (Student's T-test; $P<0.005$).

The EL4 T cell lymphoma model is particularly aggressive and known for its leaky tumor vasculature. It is one of the models in which the enhanced polymer-drug accumulation *via* EPR mechanism has been observed [204]. The cancer treatments by using free Dtxl and NPDtxl were substantially ineffective. The poor

efficacy of NPDtxl is supposed to be related to the high degree of aggressiveness of the EL4 T cell lymphoma model which is also probably insensitive to Dtxl. Additionally, the prolonged degradation time of PBSBDL (~ 2 weeks) and the favorable Dtxl-PBSBDL hydrophobic interactions leads to a slow release kinetics of the hydrophobic drug at the acidic intracellular environment of the tumor cells as evidenced and supported by the *in vitro* release data (Fig. 13).

In summary, the manufactured system combines desirable characteristics of polymeric NPs and HPMA-based polymer drug conjugates: (i) high drug encapsulation, (ii) Dox pH-triggered drug release and (iii) combinatorial chemotherapy. Simultaneous temporal controlled release of two chemotherapeutics has been achieved through the physical entrapment of Dtxl into the degradable PBSBDL copolyester core and the covalent attachment of Dox to the HPMA-based copolymer *via* pH-sensitive hydrazone bound. The cargo capacity and the relative ratio of drugs are amenable to fine tuning by varying the amount of bound drug during HPMA copolymer synthesis and NPs formulation. Multivalency of the PHPMA polymer precursor also allows attachment of targeting moieties enabling the combination of passive and active NPs targeting.

4.3 pH-responsive soft matter assemblies for cancer chemotherapy

To circumvent the drawbacks of the prolonged degradation time of PBSBDL (~ 2 weeks) and the favorable Dtxl-PBSBDL hydrophobic interactions leading to a slow release kinetic of the hydrophobic drug at the acidic cytosolic or endosome conditions in tumour cells resulting in the inefficacy of the tumor treatment (*vide* **section 4.2**., Fig. 14) pH-responsive soft matter assemblies are promising systems aiming at drug-release for cancer chemotherapy (*vide* section **2.6** and **2.6.1**).

As mentioned previously the controlled drug release can be achieved by triggering the chemical bond or by using polymers susceptible to environmental conditions (*vide* sections **2.6** and **2.6.1**), such as the acidic environment in endosomal and lysosomal compartments (*see* section **2.6.1** and Fig. 3). In such way, we recently devised block copolymers to produce NPs comprising an acid-degradable ketal labile group as a linkage between the hydrophobic poly(ε-caprolactone) (PCL) and the hydrophilic poly(ethylene oxide monomethyl ether) (MPEO) blocks (environmentally friendly blocks) being described in the **publication 3** and **4** (*see* Appendix). The aforementioned NPs undergoes a pH-induced NPs disassembly and aggregation, which is due to the hydrolysis of the acid-labile ketal linkage resulting on the PTX release being the polymer particles disintegrated into neutral degradation products.

Another strategy is by using polymers that undergoes a sharp hydrophobic-hydrophilic pH-induced transition within a pH range that is desirable for tumor-targeting drug delivery. It is the particular case of the hydrophobic PDPA block which is protonated (hydrophilised) in the narrow range of pH ($6.51 < pH < 6.85$; $\Delta pH \sim 0.34$). The PDPA block-forming core is a promising smart material for the construction of tumor-targeting drug delivery polymeric nanocarriers because it is able to encapsulate hydrophobic anticancer drugs and it undergoes a sharp hydrophobic-hydrophilic pH-induced transition within a pH range that is desirable for tumor-targeting drug delivery (described in the **publication 5,** *vide* appendix). The aforementioned features of the ketal linkage and the PDPA block copolymers are briefly described herein.

4.3.1. <u>Novel poly(ethylene oxide monomethyl ether)-*b*-poly(ε-caprolactone) diblock copolymers containing a pH-acid labile ketal group as a block linkage</u> (*publication 3***)** and **<u>pH-triggered release of paclitaxel from nanoparticles made from biodegradable block copolymer containing ketal groups between polymer blocks (</u>*publication 4*)**

A new synthetic pathway was reported for the synthesis of a novel class of well-defined biocompatible and biodegradable acid-labile MPEO-*b*-PCL diblock copolymers containing ketal groups as block linkers. The PEO and PCL polymers were chosen as building blocks since are of special interest for their environmental, biomedical and pharmaceutical applications. [42, 206, 207] PCL is an aliphatic hydrophobic polyester with great potential as biomaterial due to its unique combination of biodegradability and biocompatibility [208] and PEO is a hydrophilic and very flexible biocompatible polymer, non-toxic and easily eliminated from the body. [209] For the synthesis, a multistep efficient pathway was selected resulting in new block copolymers with reasonable yields. Different synthetic routes (*e.g.*, carbodiimide chemistry, "click" reaction and ring-opening polymerization) were applied for the preparation of low-molecular-weight compounds as precursors for building the acid-labile ketal group of the MPEO-*b*-PCL diblock copolymers (Scheme 1), herein referred to as $MPEO_{44}$-*b*-PCL_{17} and $MPEO_{44}$-*b*-PCL_{44}.

The MPEO-*b*-PCL diblock copolymers (Scheme 1, compound 7 and Table 4) were successfully synthesised by ROP from the ε-CL monomer. The previously synthesised *α*-methoxy-*ω*-hydroxy-poly(ethylene oxide) containing a ketal group (Scheme 1, compound 6) was used as a macroinitiator in the presence of $Sn(Oct)_2$ as a catalyst. The lengths of the PCL blocks were controlled by regulating the ε-CL/macroinitiator molar ratio. The newly obtained compounds (precursors, macromer, macroinitiator and final diblock

copolymers) were assessed by ^{1}H NMR, ^{13}C NMR, FT-IR spectroscopy and SEC analysis, which are described in detail, together with the full synthetic routes in the **publication 3** (*vide* Appendix).

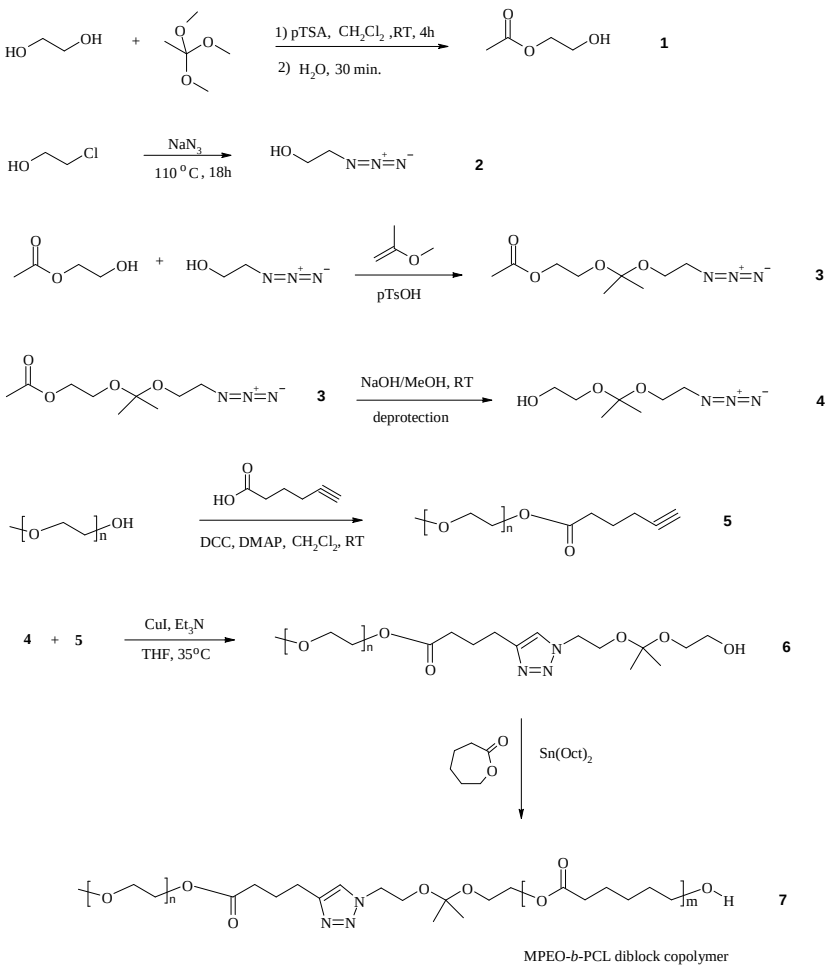

Scheme 1. Synthetic route for the preparation of MPEO-*b*-PCL diblock copolymers.

Table 4. Macromolecular characteristics of MPEO-*b*-PCL diblock copolymers.

Sample	M_n,[a] (NMR)	M_n,[b] (NMR)	M_n,[c] (SEC)	M_w/M_n,[d] (SEC)
$MPEO_{44}$-*b*-PCL_{17}	4000	5400	3130	1.45
$MPEO_{44}$-*b*-PCL_{44}	7000	6830	7570	1.43

[a] M_n was calculated by the monomer conversion; $M_n = [M]_o/[I]_o$ x 114 + M_n *α*-methoxy-*ω*-hydroxy-MPEO containing a ketal group (Fig. S1 and S2, ESI, vide Appendix). [b] M_n was calculated by ^{1}H NMR spectroscopy according to Eq. 2 (ESI, vide Appendix). [c] M_n and [d] M_w/M_n values are relative to PS standards (Fig. S3, ESI, vide Appendix).

As a proof-of-concept, polymer NPs were prepared from the block copolymers, and their behaviours under different simulated physiological conditions were evaluated in detail by DLS and nanoparticle tracking analysis (NTA). The visual appearance of the colloidal particles immediately after the injection of the MPEO-*b*-PCL block copolymer solutions into water was size-dependent and did not change after the dilution with PBS (pH ~ 7.4) (data not shown). For $MPEO_{44}$-*b*-PCL_{17}, the resulting colloidal solution was fully transparent, whereas the solution was slightly opalescent for the $MPEO_{44}$-*b*-PCL_{44} block copolymer. This result is a visual indication that the particles produced by the nanoprecipitation protocol using the $MPEO_{44}$-*b*-PCL_{44} block copolymer are larger than the particles produced using the $MPEO_{44}$-*b*-PCL_{17} block copolymer [210].

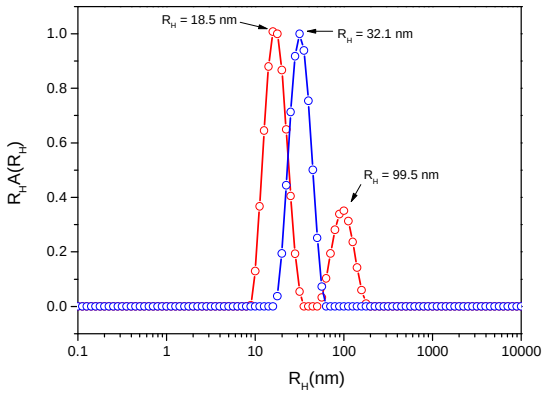

Figure 15. Distributions of R_H for (○) $MPEO_{44}$-*b*-PCL_{17} and (○) $MPEO_{44}$-*b*-PCL_{44} NPs prepared by nanoprecipitation protocol and diluted in PBS (pH ~ 7.4) both at concentration of 1 mg·mL^{-1}.

Fig. 15 shows the distribution of R_H for $MPEO_{44}$-*b*-PCL_{17} and $MPEO_{44}$-*b*-PCL_{44} block copolymer micelles after the dialysis process and dilution with PBS, as measured by DLS. The distribution of R_H for $MPEO_{44}$-*b*-PCL_{17} appears as only one single distribution of R_H relative to the presence of the polymer micelles in PBS solution with an average of R_H ~ 32.1 nm (Fig. 15, blue circles). Furthermore, the $MPEO_{44}$-*b*-PCL_{17} micelles polydispersity is very low as it was estimated by using the Cumulant analysis (μ/Γ^2 = 0.08 ± 0.007). However for the $MPEO_{44}$-*b*-PCL_{44} block copolymer a bimodal distribution of R_H was observed with average sizes of R_H = 18.5 nm and 99.5 nm respectively (Fig. 15, red circles).

The observed bimodal size distribution of R_H for the PEO_{44}-*b*-PCL_{44} block copolymer is related to morphological mixture of particles from at least two types. According to the literature [211-213], the most probable morphologic structures are the mixture between spherical micelles with an average size of D_H = 37.0 nm and cylindrical and/or worm like micelles with D_H = 199 nm. On the other hand, for PEO_{44}-*b*-PCL_{17} block copolymer assemblies of single monodisperse spherical micelles are obtained in most of the cases.

It should be noted that thermodynamically stable polymeric NPs with hydrodynamic diameters within the range of 20 to 70 nm have been shown to be ideal for tumor drug-delivery applications.[155] They are within the range enabling to avoid renal clearance (D_H > 10 nm) thus providing the NPs possibility of a prolonged blood circulation time and, considering that their size is below the cut-off size of the leaky pathological vasculature (D_H < 200 nm), also specific accumulation in solid tumor tissue due to the EPR effect. Moreover, beyond the role of the particle size in EPR effect another important aforementioned target in cancer therapy is the acidic cytosolic or endosomal conditions in tumor cells. Therefore, the sensibility of the polymer NPs containing the acid-labile ketal group was tested by DLS in acidic media (pH ~ 5.0) under simulated physiological conditions (37 °C) using the $MPEO_{44}$-*b*-PCL_{17} block copolymer. $MPEO_{44}$-*b*-PCL_{17} block copolymer NPs was chosen for evaluation of the ketal linkage sensibility *in vitro* since they presented a monodisperse single distribution of R_H with a D_H = 64.2 nm – in the range of the optimal size for drug delivery applications. The distribution of R_H for $MPEO_{44}$-*b*-PCL_{17} block copolymer NPs under pH ~ 5.0 at 37 °C and as a function of time clearly shows an increase in the average size of the micellar NPs from R_H = 32.1 nm to R_H 52.6 nm in 24 hours (*vide* Appendix, **publication 3**). This means an increase in D_H of about 41 nm. To assess a thorough size distribution and gain more information to accurately analyze the distribution of monodisperse and polydisperse samples than DLS the $MPEO_{44}$-*b*-PCL_{17} NPs were analyzed by nanoparticle tracking analysis (NTA) at 25 ºC. NTA is a powerful tool and it is particularly valuable for the detection and accurate sizing of a broad range of population ratios because it simultaneously depicts the particle size, concentration (number) and intensity distribution in the same measurement. The results show the presence of only one peak at pH ~ 7.4 (Fig. 16, left) and the presence of several peaks at pH ~ 5.0 (Fig. 16, right) mostly located at lower and larger sizes after 72 h of incubation. The broadening in particle size and size distribution as shown by NTA is an evidence of NPs disassembly and aggregation over time, which is a result of the hydrolysis of the acid-labile ketal linkage (*vide* Appendix, **publication 3**).

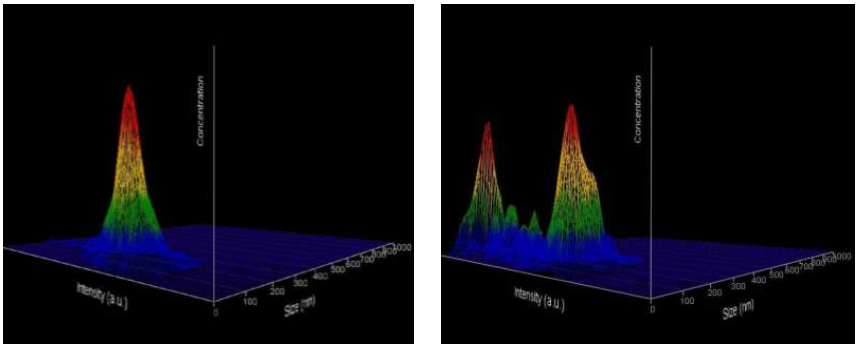

Figure 16. Size distribution as obtained from NTA for the $MPEO_{44}$-*b*-PCL_{17} NPs under pH ~ 7.4 (left) and pH ~ 5.0 (right) after 72 h.

In a similar way the TEM images (Fig. 17) show comparable increase of the $MPEO_{44}$-*b*-PEO_{17} block copolymer NPs size under pH ~ 5.0 (Fig. 17, b) when compared to the NPs under pH ~ 7.4 (Fig. 17, a) after 24 hours. Such increase in particle size and size distribution shown by both scattering techniques and TEM is a strong evidence of micellar aggregation over time. The aggregation mechanism could be explained by means of the hydrolysis of the acid-labile ketal linkage in the $MPEO_{44}$-*b*-PCL_{17} block copolymer micelles under pH 5.0. After the ketal hydrolysis takes place at the interface between the PCL core and the PEG shell inside the micelles the free hydrolyzed PEG chains start to be released in the media (*vide* Appendix, **publication 3**). The decrease in surface PEG chains density leads to a decrease in the particles steric hindrance and an increase in the particles hydrophobicity, thus, particle aggregation.

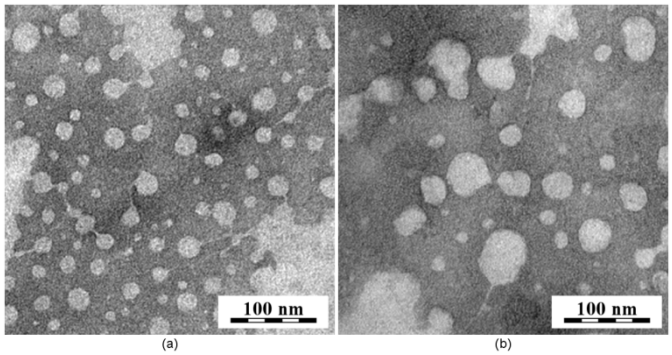

Figure 17. TEM images of $MPEO_{44}$-*b*-PCL_{17} at pH ~ 7.4 (a) and pH ~ 5.0 (b) after 24 h incubation.

Furthermore, no changes in the particle sizes distribution could be observed for $MPEO_{44}$-*b*-PCL_{17} block copolymer micelles by DLS at pH ~ 7.4 during 24 hours confirming that the particles are selective to

environment containing mild acid conditions (from pH ~ 5.0 to ~ 6.5) such as tumor tissues (*vide* Appendix of **publication 3**, Fig. S11). Moreover, the degradation of the $MPEO_{44}$-*b*-PCL_{17} diblock copolymer was confirmed by ^{13}C NMR spectroscopy. The degradation was determined based on the disappearance of the signal from the ketal linkage between the PEO and PCL blocks. The ^{13}C NMR spectra of $MPEO_{44}$-*b*-PCL_{17} copolymer (a) before and (b) after DCl addition reveals the complete disappearance of the carbon signal from ketal group linker –$OC(CH_3)_2$-O– at δ = 121.50 ppm (*vide* appendix of **publication 3**, Fig. S12). This is strong evidence that hydrolytic degradation takes place in the ketal linkage of $MPEO_{44}$-*b*-PCL_{17} diblock.

Unfortunately, the usual degradation products resulting from the acid hydrolysis of a ketal group, such as acetone,[7] could not be detected in the ^{13}C-NMR spectrum. Their signal appears hidden under ε-CL repeating units in the ^{13}C NMR. According to the ^{13}C NMR spectra no changes were observed in the signal from ε-CL repeating units after the DCl addition. The signals from the methylene carbons -CO–$(CH_2)_5$-O- (17 to 21 from δ = 20 to δ = 65 ppm) and from the carbonyl group (16 at δ = 173 ppm, related to the PCL segments remain unchanged (Fig. S12, *vide* Appendix, **publication 3**). Moreover, no new signal from side products that could derive from the hydrolysis of ester bonds related to the PCL segments was detected after the acid addition.

Subsequently, the release profile of the chemotherapeutic PTX was investigated under the same aforementioned conditions (pH ~ 5.0; 37 °C), which mimic the target acidic environment in endosomal and lysosomal compartments. The release experiments at 37 °C were conducted also at pH 7.4 to simulate conditions during transport in blood and in normal healthy tissues (Fig. 18). The drug release profile is clearly pH-sensitive. The results suggest that at pH ~ 5.0 the block copolymer NPs are activated and consequently destabilized physically (pH-triggered disassembly-aggregation, Fig. 16), thus accelerating the release of the drug. The drug cargo is released almost twice as rapidely (~ 70 %) within 72 hs at pH ~ 5.0 (mimicking intracellular environment) than at physiological conditions of pH ~ 7.4. On the other hand, at pH 7.4, ~ 36 % of the drug loaded into the NPs cores is released.

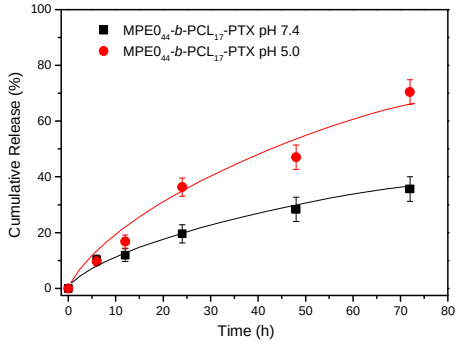

Figure 18. Paclitaxel release profiles from $MPEO_{44}$-*b*-PCL_{17}-PTX NPs at pH 5.0 (•) and 7.4 (▪).

The drug-release profile is considered not optimal; however, a yet faster release is expected in contact with more complex media such as the serum-supplied cell culture medium. Therefore, to investigate the inhibitory effect on tumor cells, the $MPEO_{44}$-*b*-PCL_{17} NPs were loaded with the antitumor drug PTX with an overall cargo content around 2.0 *wt*% (loading efficiency of 92 %, *vide* Materials and Methods, Appendix, **publication 4**). The cell viability assay was used to document *in vitro* cytotoxicity as a classical approach to evaluate the direct effect of the drug carrier NPs on target cancer cells. HeLa cell line was selected as a widely used and well-studied cancer cell model system. The drug-loaded NPs were incubated with the HeLa cells and the *in vitro* cytotoxicity after 24 h and 48 h of incubation was assessed by alamarBlue® assay (*vide* Materials and Methods, Appendix, **publication 4**).

After 48 h incubation with the cells, the PTX-loaded $MPEO_{44}$-*b*-PCL_{17} NPs exhibited significantly stronger toxicity than the free drug (Fig. 19b). In contrast, the drug-free NPs showed only negligible cytotoxicity to the cancer cells (Fig. S5, *vide* Appendix, **publication 4**). This increased cytotoxicity of the drug-carrying NPs compared to the free drug is supposedly owed to endocytotic uptake;[214] at low drug concentrations (below 1 $\mu g \cdot ml^{-1}$, see Fig. 19b) the endocytotic uptake of the drug-loaded nanocarriers would be more efficient than the uptake of free drug into the cells. With increasing drug concentration this effect becomes less prominent (*see* Fig. 19b). Once internalized *via* endocytosis the PTX-loaded nanocarriers swiftly and efficiently release their cargo, when the enzymes and acidic conditions in endosomes trigger the cleavage of the pH-sensitive acyclic ketal bond.[215, 216] Drug-free $MPEO_{44}$-*b*-PCL_{17} NPs were also tested up to the applied maximal concentration (0.67 $mg \cdot mL^{-1}$) with no significant cytotoxic activity (Fig. S5, *vide* Appendix, **publication 4**).

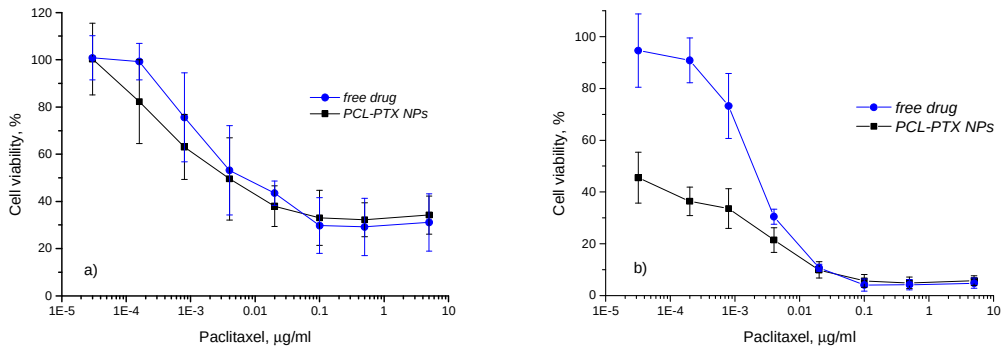

Figure 19. Cell viability of HeLa cell line after 24 h (a) and 48 h (b) of incubation with different concentrations of free PTX (blue circles) and PTX-loaded $MPEO_{44}$-*b*-PCL_{17} (black squares) NPs.

Last but not least, the negligible toxicity of the unloaded-MPEO$_{44}$-*b*-PCL$_{17}$ NPs emphasized that the presented nanocarrier system produces no toxic degradation products; and at any rate the products (PCL and PEO) are well-known FDA-approved constituents as environmentally friendly blocks.

In summary, well-defined nanoparticles prepared from the assembly of the new amphiphilic MPEO$_{44}$-*b*-PCL$_{17}$ block copolymer were presented. The NPs structure was characterized in detail by DLS, SLS, NTA and TEM. On decreasing pH the acid-labile ketal linker enabled the disassembly of the nanoparticles in a buffer that simulated the acidic environment in endosomal and lysosomal compartments. As a result the chemotherapeutic paclitaxel was released and the polymer particles disintegrated into neutral degradation products as confirmed by SEC and ^{13}C NMR and by in *in vitro* cell viability tests. In addition, the *in vitro* cell viability experiments demonstrated the great potential of the pH-triggered NPs as drug-delivery system in cancer therapy; the *in vitro* cytotoxicity studies showed an important increase in activity of the NP-loaded with drug and the drug-free NPs are degraded into well-known and FDA-approved by-products that introduce no toxicity to cells. The particle size below the cut-off size of the leaky pathological vasculature (NPs sizes < than 100 nm) and the ability to release a drug at the endosomal pH with concomitant high cytotoxicity makes them suitable candidates for cancer therapy especially *via* EPR effect.

4.3.2. Nanoparticles of the poly([*N*-(2-hydroxypropyl])methacrylamide)-*b*-poly[2-(diisopropylamino)ethyl methacrylate] diblock copolymer for pH-triggered release of paclitaxel (*publication 5*)

The potential of self-assembled NPs containing the tunable pH-responsing property of the hydrophobic PDPA core and the protein repellence of the hydrophilic PHPMA shell on *in vitro* cytostatic activity has been explored on cancer cells. The amphiphilic diblock copolymer poly[*N*-(2-hydroxypropyl)methacrylamide]-*b*-poly[2-(diisopropylamino)ethyl methacrylate] (PHPMA-*b*-PDPA) dissolved in organic solvent (ethanol/dimethylformamide) undergoes nanoprecipitation in phosphate buffer saline (PBS, pH ~ 7.4) and self-assembles into regular spherical NPs after solvent elimination. The block copolymer comprising the hydrophobic PDPA and the hydrophilic PHPMA blocks favours the formation of stable NPs with a bulky core capable of encapsulating and controlling the release of the hydrophobic chemotherapeutic PTX (discussed hereafter).

The block copolymer was prepared using RAFT polymerisation. A first block of PHPMA, M_n = 3 600 g·mol^{-1}, M_w/M_n = 1.07; Scheme 1, Fig. S1 and S2, *vide* **publication 5**) was synthesised and used as macro chain

transfer agent (macroCTA). Subsequently a long second block of PDPA (M_n = 26 200 g·mol^{-1}, M_w/M_n = 1.29) was grown from the macroCTA also by RAFT. RAFT polymerisation accounts for excellent living characteristic in the polymerization of methacrylamides.

The markedly narrow window of pH at which the DPA block copolymer can be protonated makes the block a challenge which is perfectly suitable for an effective endosomotropic (Fig. 3) delivery and outperforms many of the systems previously proposed. Figure 20 depicts the pH-triggered behaviour of the PDPA segment due to the protonation of the tertiary amino group.

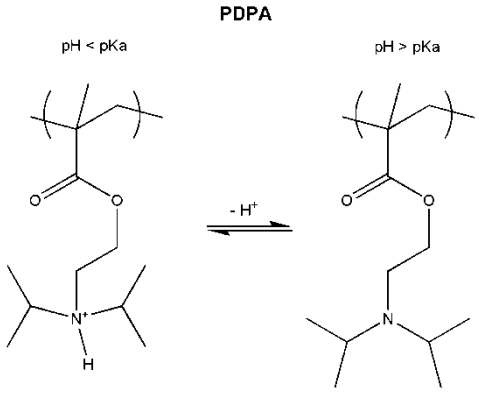

Figure 20. The pH-triggered behaviour of the PDPA segment.

The pH-triggered behavior of the block copolymer (protonation of the tertiary amino group) is also observed due to the changes in the scattering intensity and ζ-potential during the titration of the block copolymer (Fig. 21a); the pH dependence of the hydrodynamic diameter (Fig. 21b) suggests that the pH is a remarkably effective and precise trigger for assembly and disassembly of the system. The hydrophobic DPA block becomes protonated (hydrophilised) in the narrow range of pH ($6.51 < pH < 6.85$; $\Delta pH \sim 0.34$, Fig. 21a).

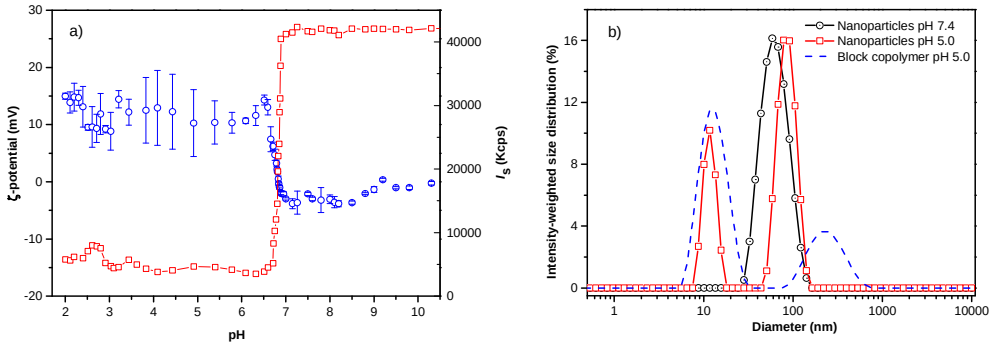

Figure 21. (a) Potentiometric acid-base titration curve for the $PHPMA_{25}$-*b*-$PDPA_{106}$ block copolymer as a function of overall scattering intensity (red squares) and zeta potential values (black circles) and (b) intensity-weighted size distribution for the $PHPMA_{25}$-*b*-$PDPA_{106}$ NPs at pH 7.4 (black circles) for the nanoparticles at pH 5.0 (red squares) and the single block copolymer at pH 5.0 (blue dashed lines); scattering angle 173°, concentration of 1 mg·mL^{-1} diluted in PBS at 37 °C.

The NPs were prepared by the solvent-shifting method, whereby $PHPMA_{25}$-*b*-$PDPA_{106}$ block copolymer was dissolved in ethanol or dimethylformamide (concentration ~ 1 mg·mL^{-1}) and phosphate buffer saline (PBS, pH ~ 7.4) was added dropwise to the organic solution under stirring until the aqueous weight fraction reached twice the weight of the organic phase. The organic solvent was removed by dialysis or evaporated under reduced pressure. The NPs structure was characterized in detail by DLS, SLS, ELS, SAXS and cryo-TEM ; the methods and results are fully described in the **publication 5** (*vide* Appendix).

DLS measurement of the diblock copolymer (before NP formation) in ethanol shows that most chains were fully dissolved with an average hydrodynamic diameter of $2R_H$ = 9.0 nm (Fig. 21b). After PBS addition and solvent evaporation the DLS shows a monomodal average size distribution referred to the NPs population ($2R_H$ = 52 nm, Fig. 21b, black circles) with low dispersity as was estimated by using the cumulant analysis (μ^2/Γ^2 = 0.120 ± 0.009), and as observed by Cryo-TEM (Fig. 22a). At pH ~ 7.4 (PBS buffer) the average ζ-potential for the studied block copolymer nanoparticles is close to neutrality (ζ ~ -2.5 mV) (Fig. 21a). Decreasing the pH below the pKa (DPA) (6.51 < pH < 6.85) the system is rapidly protonated as evidenced by the positive ζ-potential and mainly composed of molecularly dissolved block copolymer chains besides a very small number of large aggregates (R_H ~ 125 nm). Cryo-TEM images obtained at pH ~ 7.4 reveal well-defined spherical NPs (Fig. 22). The PHPMA chains at the outermost layer of the particles couldn't be evidenced by cryo-TEM image due to poor contrast.

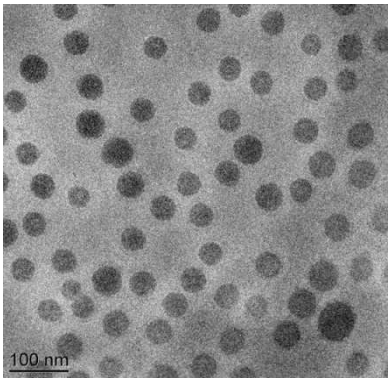

Figure 22. Cryo-TEM image of the block copolymer NPs in PBS, pH ~ 7.4.

As already mentioned, the long-term stability of the NPs in serum is a pre-requisite for the use of polymer NPs *in vivo* because the efficient NPs accumulation in the solid tumor tissue requires an extended circulating capability to enable a time-dependent extravasation of the NPs through the EPR effect (Fig. 3a, *vide* Appendix, **publication 5**) shows the temporal stability of the NPs in diluted human blood plasma as a function of the incubation time by evaluating their detrimental interaction with proteins from blood (human plasma, 10% diluted in PBS).

The PHPMA chains prevented the fouling of proteins resulting in a remarkable stability of the NPs in serum. The size and scattering intensity patterns of the NPs do not change within the studied 36 h suggesting that the NPs are stable in the simulated but highly challenging media. The high stability of the NPs is based on their hydrophilic shell nature-improved colloidal stability-and by its unmatched resistance to protein adsorption. [88, 155, 217] By preventing any adsorption of proteins the NPs are virtually “invisible” for the blood millieux, which makes them a promising system for *in vivo* applications. [81, 155, 218]

Subsequently, the release profile of the chemotherapeutic PTX was investigated under conditions mimicking the acidic environment in endosomal and lysosomal compartments, pH ~ 5.0 and 37 °C. The release experiments at 37 °C were conducted also at pH 7.4 to simulate conditions during transport in blood and in normal healthy tissues (Fig. 23). The drug release profile is clearly pH-sensitive in accordance with the physico-chemical studies presented above.

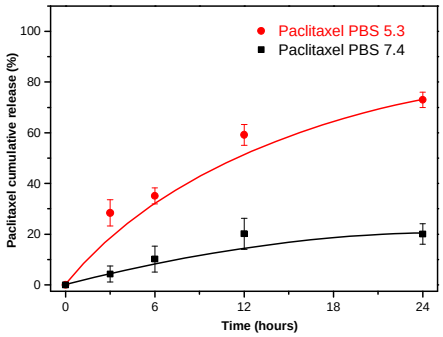

Figure 23. Drug release profiles from paclitaxel-loaded PHPMA$_{25}$-*b*-PDPA$_{106}$ block copolymer NPs at pH 7.4 (PBS, closed black squares) simulating transport in blood and at pH 5.3 (PBS, closed red circles) simulating the acidic environment in endosomal and lysosomal compartments at 37 °C.

The results suggest that at pH ~ 5.0 (acidic environment in endosomal and lysosomal compartments) the block copolymer becomes protonated: becomes a polycation. The Coulombic repulsion among the chains disrupts the NPs which physically disassemble (pH-triggered disassembly, Fig. 21 and 23), thus resulting in a 3.5 fold acceleration of the rate of release of the chemotherapeutic (~ 70 %) within 24 h, (pH ~ 5.0) compared to physiological conditions (PBS). Besides that, ~ 21 % of the drug was released from the intact NP cores when kept in PBS at pH 7.4.

The release data demonstrate that during the systemic circulation minimal quantity of the drug would be released before reaching the solid tumor environments *via* the EPR effect. Conversely, the chemotherapeutic is readily released at pH 5.0 with ~ 70 % of the loaded anticancer drug released within first 24 h fulfilling the criteria [219] for a pH-triggered drug release mechanism exhibiting practical application as nanocarriers in passive tumor-targeted drug delivery.

Finally, to investigate the inhibitory effect on tumor cells, the pH-triggered PHPMA$_{25}$-*b*-PDPA$_{106}$ NPs were loaded with the antitumor drug PTX with an overall cargo content around 2.5 *w*t % and a loading efficiency of 96 % (*vide* Appendix, **publication 5**). The cell viability assay using alamarBlue® was used to examine the *in vitro* cytotoxicity as a classical approach to evaluate the direct effect of the drug-loaded NPs on target cancer cells. The HeLa cell line was selected as a widely used and well-studied cancer cell model system. The drug-loaded NPs were incubated with the HeLa cells for 24 and 48 h. The *in vitro* cell viability experiments demonstrated that the PTX-loaded-PHPMA$_{25}$-*b*-PDPA$_{106}$ NPs exhibited a similar if not slightly stronger cytotoxic effect as the free drug after 24 h of incubation (Fig. 24a). After the incubation over 48 h the superior toxicity of the PTX-loaded-PHPMA$_{25}$-*b*-PDPA$_{106}$ NPs compared to free PTX is clearly visible (Fig. 24b). The

NPs (IC_{50} 0.1 ng·mL^{-1}) exhibited significantly higher cytotoxicity than the free PTX (IC_{50} 1.7 ng·mL^{-1}) which corresponds to values stated in the literature for HeLa cells. [220, 221]

This increased cytotoxicity of the drug-carrying NPs compared to the free drug has been previously reported for analogous systems [66, 222, 223] and is supposedly the result of enhanced endocytotic uptake of NPs. In particular at low drug concentrations and higher incubation times (below 0.005 µg·mL^{-1}, Fig. 24b) the endocytotic uptake of the PTX-loaded NPs is more efficient than the uptake of free drug into the cells. [222] A strong toxicity of the drug-loaded NPs after 48 h incubation correlates with the hypothesis that a significant amount of particles is already internalized in endosomal compartments within the first 24 h – and that this is closely followed by a fast release of the drug (within 24 h approx. 70% of the drug was released under acidic conditions mimicking conditions in endosomal and lysosomal compartments, see Fig. 23). Drug-free PHPMA$_{25}$-*b*-PDPA$_{106}$ NPs were also tested up to the applied maximal concentration (0.4 mg·mL^{-1}) with no significant cytotoxic activity (Fig. 24a and 24b, Fig. S4a and Fig. S4b, *vide* Appendix, **publication 5**).

It is important to highlight that the extracellular pH differences between the tumoral tissues and the healthy tissues are not just a characteristic of tumors but also ischemia, imflammation, renal failure or chronic obstructive pulmonary diseases that share also similar pH differences to their healthy counterparts. Therefore the HPMA-*b*-PDPA copolymer NPs may also find applications as drug carriers for their treatment.

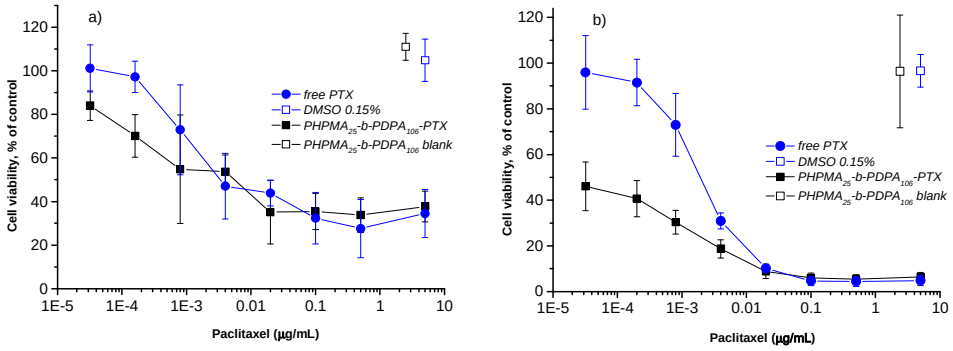

Figure 24. Cell viability of HeLa cell line after 24 h (a) and 48 h (b) incubation with different concentrations of free PTX (closed blue circles) and PTX-loaded PHPMA$_{25}$-*b*-PDPA$_{106}$ (closed black squares) NPs. DMSO 0.15% (open blue squares) and blank PHPMA$_{25}$-*b*-PDPA$_{106}$ NPs (open black squares) were used as controls.

In summary a diblock copolymer of PHPMA and PDPA was prepared by RAFT polymerisation. The diblock copolymer was assembled into spherical NP consisting of a core of PDPA and a corona of PHPMA as

evidenced by SLS, cryo-TEM and SAXS. Presumably, the PHPMA chains prevented the fouling from proteins resulting in a remarkable stability in serum. Reduction of the pH below 6.85 resulted in a rapid increase in the zeta-potential and the fast disassembly of the particle (size decrease as observed by DLS). This was exploited as a trigger for the delivery of hydrophobic drugs into cancer cells. Minimal amount of drug was released above the threshold pH. The *in vitro* cytotoxicity studies showed an important increase in activity of the NP loaded with drug compared to the free drug.

The particle's size below the cut-off size of the leaky pathological vasculature ($2R_H$ < 100 nm), the excellent stability in serum and the ability to release a drug at the endosomal pH with concomitant high cytotoxicity makes them suitable candidates for cancer therapy, namely for treatment of solid tumours exhibiting high tumor accumulation of NPs due to effective EPR effect.

4.4. ROS-responsive soft matter assemblies for cancer chemotherapy

4.4.1 Fluorescent boronate-based polymer nanoparticles with reactive oxygen species (ROS)-triggered cargo release for drug delivery applications

(*publication 6*)

The incorporation of selectively chemically degradable linkages into polymer-based nano (NPs)- and microparticulate drug-delivery systems allows to achieve external stimulus-triggered polymer degradation and triggered release. [10, 224, 225] This is a very useful feature both to release the therapeutic cargo and to eliminate the biomaterial from the body after the cargo is released and the carrier is no longer needed. Such stimulus may be an enzymatic removal of protecting groups, a pH change, light or more recently, the presence of reactive oxygen species (ROS) in the surrounding environment (*vide* section **2**.**6**.**2**). [226-228] The ROS play a crucial role in human physiological and pathophysiological processes. An increasing amount of data indicates that ROS such as, *e.g.*, H_2O_2, is a component of cell signaling pathways that are necessary for the growth, development, and fitness of living organisms. [229] On the other hand, imbalances in H_2O_2 production lead to oxidative stress and inflammation events, which damage tissue and organ systems and are correlated with the onset and advancement of various diseases, including cancer, diabetes, cardiovascular and neurodegenerative diseases. [230-233] Several works suggest that many human cancer cells show higher H_2O_2 levels compared to their normal counterparts. [234-238] Specifically, H_2O_2 has become a common marker for oxidative stress playing important roles in carcinogenesis and is also linked to *e.g.*, apoptosis, cell proliferation and DNA

mutations. [239-241] Thus the involvement of ROS in cellular signaling and disease states has motivated the construction of clever chemical tools as ROS-responsive micro- and NPs as drug carriers. [242-244]

The ability to generate a triggered nanoparticle carrier response (*e.g.*, release of cargo or polymer degradation) in ROS rich microenvironments is of particular interest, *e.g.*, for the targeted drug delivery to tumors and sites of inflammation (*vide* section **2.6.2**). [226, 227, 243-245]

Herein, a biocompatible and biodegradable ROS-sensitive polymer backbone with the capability of cellular imaging to ROS-rich environment was synthesized by step-growth polymerization from monomers bearing a ROS-degradable pinacol-type boronic ester and alkyne moiety suitable for click chemistry-based attachment of active cargo (Scheme 2).

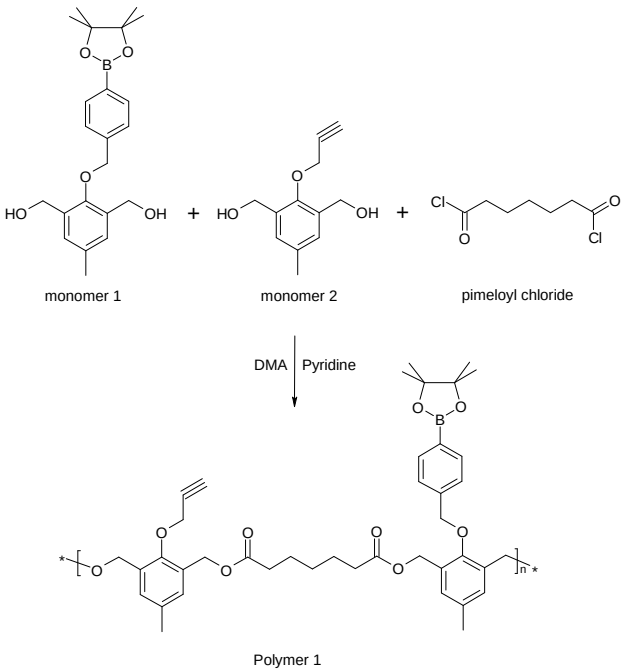

Scheme 2. Synthesis of the ROS responsive polymer bearing the universal monomer 2 for click reaction.

Initially, monomer 1 was synthesized according to the previously reported procedure[243] (ESI, *vide* Appendix, **publication 6** for synthetic route). Monomer 2 (Scheme 2) was synthesized by the protection of 2,6-bis-(hydroxymethyl)-p-cresol with tert-butyldimethylsilyl chloride generating the compound 2 that was then reacted with propargyl bromide to provide the protected alkyne compound 3 (Fig. S1, *vide* Appendix, **publication 6**).

The monomer 2 (Scheme 2) was obtained in high yield (94 %) after the removal of the protecting groups from compound 3 (Fig. S2, *vide* Appendix, **publication 6**). The synthesized monomers 1 and 2 were

further successfully copolymerized with pimeloyl chloride generating the ROS-responsive polymer 1 (P-1) (Scheme 2 and *vide* Appendix, **publication 6**). Successful polymer synthesis was confirmed by the ^{1}H NMR (Fig. 25) and by SEC analysis (Fig. 26 - right). Weight-average molecular weight (M_w) of polymer P-1 was 21.5 kDa with reasonable polydispersity index PDI = M_w/M_n = 1.49 (where M_n is the number-average molecular weight) as determined by SEC (Fig. 26, right). The ^{1}H NMR spectrum of P-1 shows characteristic signals for protons belonging to the repeating units of monomers. The signals from protons in monomer 1 and monomer 2 aromatic rings were detected at δ = 7.68 ppm (1 - *vide* Fig. 25 for signal-structure assignment), δ = 7.41 ppm (2), and δ = 7.16 ppm (3). The methylene protons (4) of monomers 1 and 2 from the main chain of P-1 where observed in the same position at δ = 5.08 ppm, whereas the signals attributed to the methylene groups of side chains of monomers 1 (5) and 2 (6) appear at δ = 4.88 and 4.57 ppm, respectively (Fig. 25). The signal of the proton of the terminal alkyne group (7) is at δ = 2.51 ppm (spectrum of P-1 in d_6-DMSO is given also, Fig. S3, *vide* Appendix, **publication 6**). Furthermore, the spectrum displayed signals of methylene groups (10) from pimeloyl chloride monomeric repeating unit at δ = 1.48 ppm, and peaks of the methyl with methylene groups (8 + 9, 12 + 11) with chemical shift at δ = 2.25 and 1.26 ppm, respectively. A ROS-insensitive counterpart to the P-1 polymer (polymer 2; P-2) was also synthesized to investigate the ROS response to the intracellular drug release efficiency. Spectra of the ROS-insensitive counterpart polymer 2 in $CDCl_3$ showed the characteristic peaks (Fig. S4, *vide* Appendix, **publication 6**), which also indicated successful polymer synthesis.

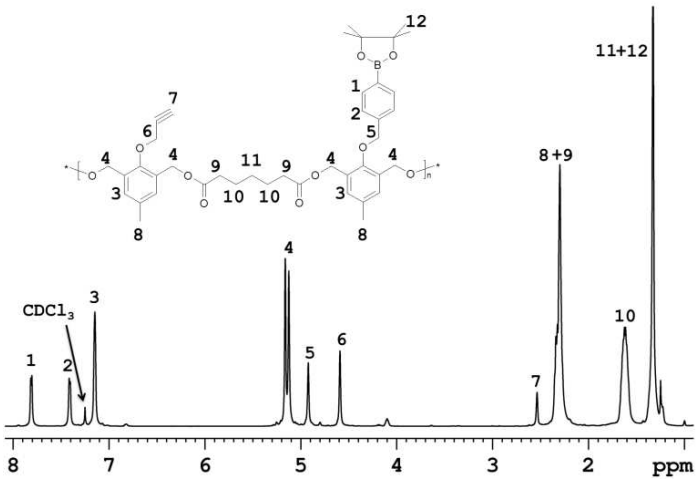

Figure 25. ^{1}H NMR spectra of the synthesized ROS-responsive polymer (P-1) containing the monomer 2 units enabling the polymer modification by click reaction in $CDCl_3$.

The degradation of the P-1 polymer in presence of H_2O_2 was characterized by SEC analysis and ^1H NMR following the modified methodology according to Almutairi *et al.*, 2012. [243] In a typical experiment, the P-1 was incubated in a 20% PBS/DMF (*v*/*v*) solution containing different H_2O_2 concentrations and at predetermined time intervals aliquots were examined by SEC (*vide* Appendix, **publication 6**). The SEC chromatogram (Fig. 26, right) shows that P-1 degraded into small molecules and oligomers in a time- and H_2O_2-dependent manner. Polymer degradation proceeds more extensively with increasing incubation time and H_2O_2 concentration. P-1 was shown to be responsive to physiological levels of H_2O_2 (< ~ 1 mM) [247] after 1 day of incubation (Fig. 26 - right) while the non-ROS-responsive counterpart polymer (P-2) showed almost no degradation (data not shown).

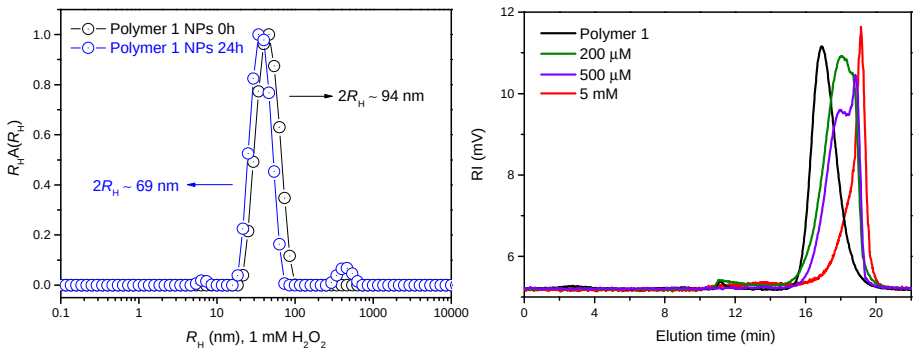

Figure 26. Distributions of R_H for P-1 (○) prior the H_2O_2 addition and (○) after 24h of incubation in 1 mM of H_2O_2 (left) and SEC chromatograms of P-1 prior to the addition of H_2O_2 (black line) and after degradation in 20% PBS/DMF solutions containing 200 µM, 500 µM and 5 mM of H_2O_2 incubated at 37 °C for 1 day (right).

When degradation of both polymers was compared at higher H_2O_2 concentrations and for longer time (5 mM, 4 days), degradation of P-2 polymer was only partial (Fig. S5, *vide* Appendix, **publication 6**). The degradation of the polymer P-1 evaluated with ^1H NMR was complete after 5 days of incubation (Figure 27) as broad peaks in ^1H NMR related to polymer are replaced by sharp peaks of the low-molecular-weight degradation products (monomers) confirming the depolymerisation of the P-1 triggered by the H_2O_2 (Fig. 27).

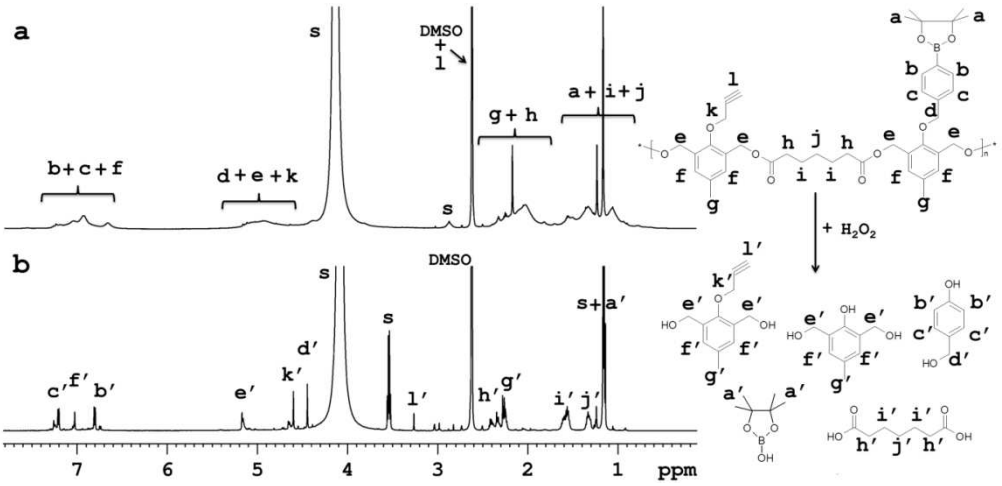

Figure 27. ^{1}H NMR spectra of polymer 1 in d_6-DMSO, deuterium PBS (a) without H_2O_2 and (b) incubated with 50 mM H_2O_2 after 5 days at 37 °C. "s" refers to solvent peaks (HDO in D_2O and ethanol).

From the P-1 and P-2 polymers NPs were prepared by a nanoprecipitation protocol (*vide* Appendix, **publication 6**) and their behavior under simulated physiological ROS concentrations (1 mM of H_2O_2) was evaluated in detail by DLS, SLS, TEM and by *in vitro* drug model release experiments. Note that the NPs were prepared with hydrodynamic radius ($2R_H = D_H \sim 94$ nm), *e.g.*, within a range known to be ideal for efficient tumor accumulation due to the EPR effect. [248] The ROS-responsiveness capability of the P-1 NPs was tested by DLS after 24 h of incubation with 1 mM of H_2O_2. The Fig. 26 (left) shows the distribution of R_H for P-1 NPs prior and after 24 h of incubation as measured by DLS. The distribution of R_H for P-1 NPs appears as only one single distribution of R_H relative to the presence of the single spherical polymer NPs in PBS solution with an average diameter of $2R_H \sim 94$ nm (Fig. 26, black circles - left). Furthermore, the polydispersity of the NPs is very low as estimated through the Cumulant analysis ($\mu/\Gamma^2 = 0.08 \pm 0.007$) (*vide* Appendix, **publication 6**). This is important for the homogeneous biological behavior of such NPs. However, after 24 h of H_2O_2 incubation, a trimodal distribution of R_H was observed. In addition to the NPs peak, the presence of molecularly dissolved copolymer chains as well as a peak of large aggregates with loose structure could be noticed in the aqueous solution at 1 mM of H_2O_2. Three well-defined peaks highlighting the three populations of the scattering polymer with average diameters of $D_H \sim 11$ nm, 69 nm and 1.9 µm were identified (Fig. 26, blue circles - left). They can be attributed to free chains and their fragments, surface-eroded nanoparticles (decrease in D_H of ~ 25 nm) and polymer aggregates, respectively. [10, 88] Further the polymer degradation-triggered cargo release was studied using the release of the fluorescent model of a drug, the Nile Red (NR). The NR-loaded ROS-responsive (from

polymer P-1) and non-ROS-responsive (from polymer P-2) NPs were examined with fluorescence spectroscopy measurements along 24 h of incubation with 1 mM of H_2O_2 (Fig. 28). After 24 h the NR release from the ROS-responsive NPs was almost ~6 times faster than the NR release from their non-ROS-responsive counterparts, thus confirming the potential of the P-1 polymer NPs to release the model drug specifically in simulated ROS-rich microenvironments (Fig. 28).

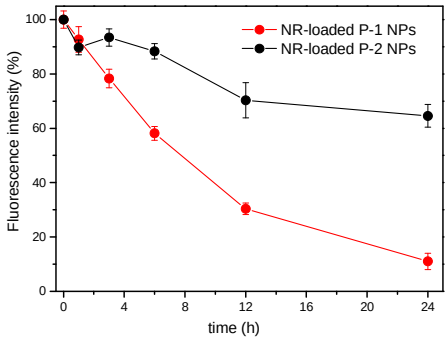

Figure 28. Nile Red (NR) release from ROS-responsive polymer NPs (P-1) and from polymer counterpart NPs (P-2) after the incubation with 1 mM of H_2O_2 along 24 h.

The polymer NPs degradation was also investigated through TEM (Fig. 29). The TEM microscopy showed particle size qualitatively comparable to that determined by DLS (Fig. 26, left). Prior to incubation with H_2O_2, compact NPs of spherical morphology and narrow size distribution ($D_H \leq 85$ nm) were observed (Fig. 29). After incubation with 1 mM of H_2O_2, the NPs showed diffuse irregular shapes and a very broad size distribution, with the smallest NPs well below 10 nm and the largest NPs above ~ 100 nm (Fig. 29b). This suggested that H_2O_2 caused decomposition of the NPs, and the decomposed parts were probably re-agglomerated due to their hydrophobicity. SLS data support the findings that the NPs underwent surface degradation as well as core decomposition, as the particles' D_H decreased (by 25 nm, see Fig. 26, left) as well as the overall scattering intensity (Fig. S10a, *vide* Appendix, **publication 6**) followed by the increase in particles R_G (gyration radius), a characteristic of core hydration and swelling of the scattering particles in solution (Fig. S10b, *vide* Appendix, **publication 6**) [69, 249, 250]

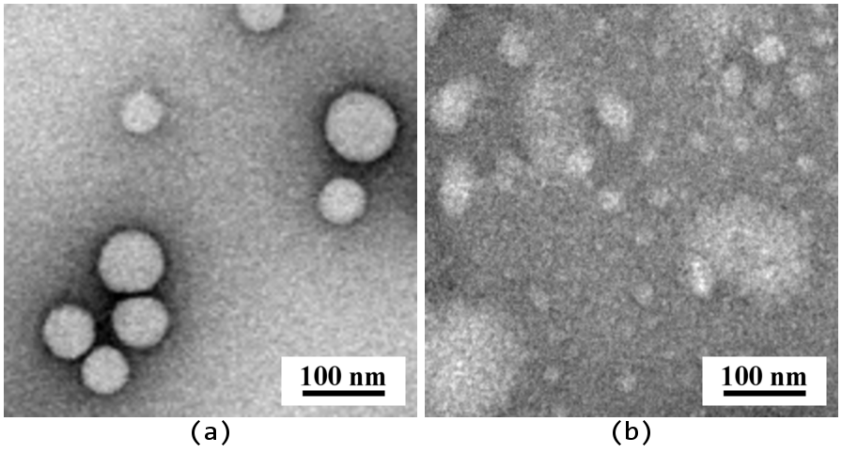

Figure 29. TEM micrographs of polymer NPs prior the incubation with H_2O_2 (a) and after 48 h of incubation with 1 mM of H_2O_2 (b).

The decomposition was also in agreement with the observed low contrast for the incubated NPs (Fig. 29b). Compact NPs exhibited sharp edges and high contrast, whereas decomposed NPs, NPs fragments and their agglomerates showed only a vague interface.

The cellular uptake of P-1 and P-2 NPs loaded with NR (dye loading ~ 0.2 wt.%, Fig. S7 and S8, *vide* Appendix, **publication 6**) and the intracellular NR release were followed *in vitro* in human prostate cancer (PC3) cells (for method, *vide* Appendix, **publication 6**). The latter are known to produce high ROS levels. [251] While inside the particles the NR fluorescence is strong, upon ROS-triggered NPs degradation in cells the dye will be released and get quenched outside the NPs (due to polarity changes in the micro-surrounding). After 4 h both NPs displayed similar fluorescence intensity in the cells, however, after 20 h the fluorescence of P-1 was lower compared to P-2 (Fig. 30, bellow). This indicated faster ROS-triggered degradation of P-1 NPs after prolonged exposure in ROS-producing cells.

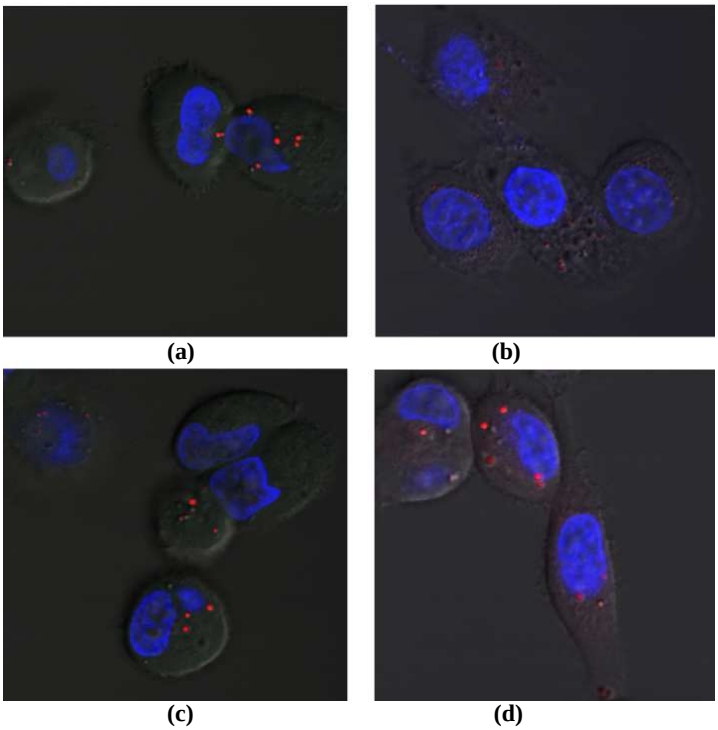

Figure 30. Confocal microscopy images of Nile Red-loaded P-1 NPs (a,b) and P-2 NPs (c,d) in PC3 cells after incubation for 4 h (a,c) and 20 h (b,d) at 200 $\mu g \cdot mL^{-1}$ polymer concentration. Blue - the Hoechst-stained nucleus; red - the NR.

Based on the similar uptake rate of the NPs (as also confirmed by flow cytometry, Fig. S12, *vide* Appendix, **publication 6**), the ROS-mediated fluorescence decay and cargo release of P-1 particles were further pursued *via* fluorescence lifetime microscopy (FLIM) and flow cytometry (FC). In a quantitative study *via* FC the NR quenching of the particles was evaluated in PC3 and human fibroblast (HF) cells (for methods, *vide* Appendix, **publication 6**). The latter are known for their low levels of ROS production contrary to *e.g.*, PC3. [251-254] The cells were loaded with P-1 NPs, washed and incubated for 4 h, thus exposing the internalized NPs to intracellular ROS insofar as present in the cells. Data showed that after incubation the NR fluorescence was significantly reduced in PC3 cells compared to the HF cells (Fig. 31). By the same experimental setup the Nile Red quenching of P-1 and P-2 NPs in PC3 cells was compared. In line with the previous image a lowered NR fluorescence of P-1, by a factor 0.7, compared to P-2 was observed.

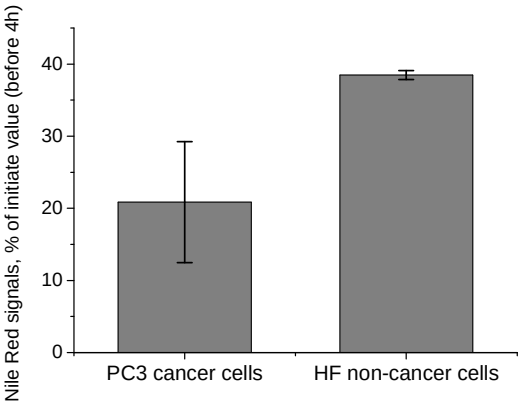

Figure 31. Nile Red fluorescence signals from NR-loaded P-1 NPs in PC3 (left) and HF (right) cells after 4 h of incubation. At t0 prior to incubation, the cells were loaded with P-1 NPs with a 2 h pre-incubation step, then the NPs were washed off (for methods, *vide* Appendix, **publication 6**).

In conclusion, the FC data acquired in PC3 cancer cells and non-cancer HF cells indicated a ROS-induced degradation of P-1, and demonstrated the polymer's potential to specifically trigger the cargo release in ROS-containing intracellular environment. As the released NR inside the cells can interact with hydrophobic cell structures and partially recover fluorescence, released NR is never fully quenched and some residual fluorescence can be visualized in microscopy.

To show the NR release *via* co-localization in FLIM microscopy, a second dye Alexa Fluor® 647 (Alx647) azide was covalently bound to the clickable alkyne linker of the P-1 *via* click reaction (Fig. S13 and S14, *vide* Appendix, **publication 6**). NR was physically entrapped into the Alx647-labeled NPs as described previously. With two fluorophores the intracellular fate of cargo (NR) and the polymer (stained covalently with Alx647) could be tracked independently. The two dyes were visualized after separate excitation at 485 nm (NR), and 640 nm (Alx647). The co-localization of P-1 NPs and the NR cargo after 8 h incubation in PC3 (Fig. 32a and 32b) and HF cells (Fig. 32c and 32d) was compared.

Analysis of lifetime τ (for method, *vide* Appendix, **publication 6**) clearly differentiated the free Nile Red (τ 4.2 ±0.3 ns, exc. at 485 nm) from the particles marked with Alx647 (τ 2.2 ±0.1 ns, exc. at 640 nm). In PC3 cells the cytoplasm was nearly homogeneously colored with the released NR (Fig. 32a), while the polymer was clustered up in few locations (Fig. 32b). Oppositely in HF cells only little homogeneous NR fluorescence was visible outside the NPs (Fig. 32c), and the NR co-localized with the polymer to a high extent (Fig. 32d). However, after 8 h even in ROS-producing PC3 cells the NPs likely were not fully degraded and the cells still contained some Nile Red as well (*vide* Appendix, **publication 6**).

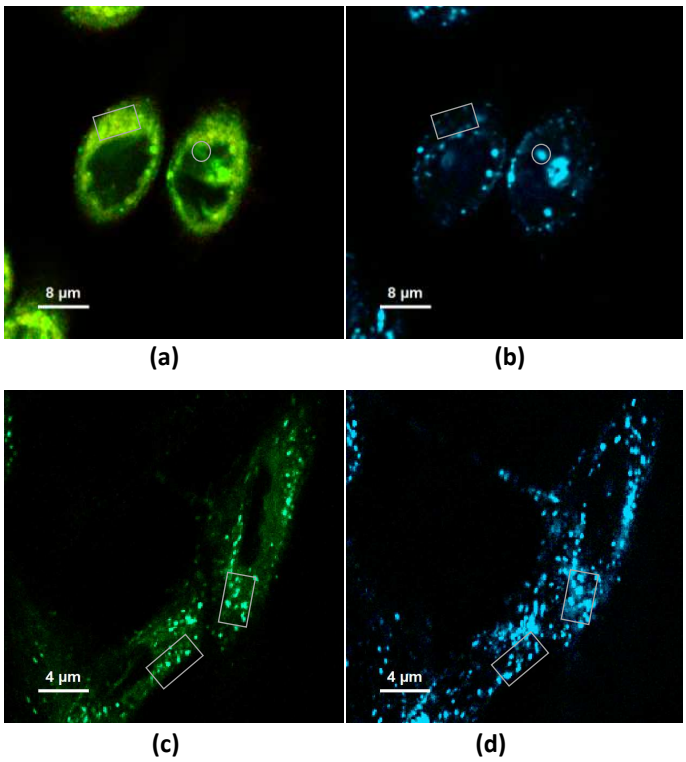

Figure 32. FLIM microscopy of dual-marked P-1 NPs in PC3 (a, b) and HF (c, d) cells after 8 h incubation, visualizing (released) Nile Red and polymer-bound Alx647. Fluorescence was detected after separate excitation at 485 nm (Nile Red, in a, c) and 640 nm (Alx647, in b, d). In a, b locations with high polymer content but little co-localizing NR are pointed out (circle), and *vice-versa* (square). In c, d the fluorescence patterns predominantly co-localize (squares).

In line with the findings after separate excitation, after simultaneous excitation at 485 nm and 640 nm the spread fluorescence of released NR was visible in PC3 but barely in HF cells, and the co-localization of not-yet released NR with the particles was visible in HF but not in PC3 cells (Fig. 33a and 33b). Furthermore, in FLIM analysis of PC3 cells after only 1 h incubation with dual-marked P-1 NPs, polymer and Nile Red were highly co-localizing and only little released, and freely distributed Nile Red was observed (Fig. 34). This evidences that the P-1 polymer NPs can be used for selective cargo release to PC3 cancer cells, with the release rate in non-cancer HF cells being lower than in the cancer cells with higher ROS levels.

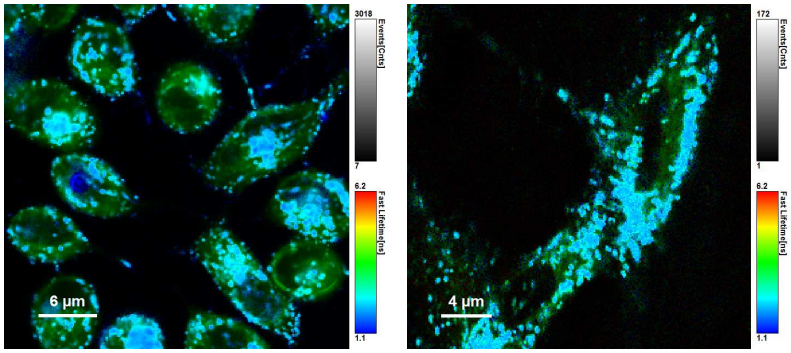

Figure 33. FLIM images of PC3 (a) and HF (b) cells after 8 h incubation with dual-marked P-1 NPs, color-coded by the averaged obtained lifetime per pixel. The localization of polymer (covalently bound Alx647, tau ca 2.2 ns, shown in blue) and of released Nile Red (spread throughout the cell, tau ca 4 ns, shown in green), and local overlap of lifetimes (turquoise tones) was visualized after simultaneous excitation at 485 nm and 640 nm.

Finally, to investigate the inhibitory effect on tumor cells, the ROS-responsive (P-1) and non-responsive counterpart (P-2) NPs were loaded with the antitumor drug paclitaxel (PTX) with an overall cargo content ~ 2.2 wt% and a loading efficiency of 94 % (*vide* Appendix, **publication 6**). The alamarBlue® viability assay was used to evaluate the cytotoxicity of the PTX-loaded P-1 and P-2 NPs in cancer cell lines and in HF cells. For this study various cancer cell lines, which are known for increased ROS production, such as human cervix carcinoma (HeLa), [254] colorectal adenocarcinoma (DLD1) [255] and prostate cancer (PC3) [251] cells were used and the NPs cytotoxicity compared with that found for the HF fibroblasts cells as low ROS controls (for methods, *vide* Appendix, **publication 6**).

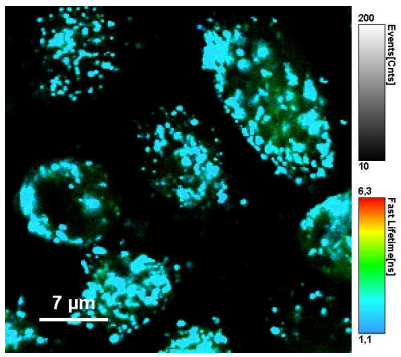

Figure 34. FLIM images of PC3 cells after 1 h incubation with dual-marked P-1 NPs, color-coded by the averaged obtained life-time per pixel. The localization of polymer (covalently bound Alx647, tau 2 ns, shown in blue) and of Nile Red (originally physically entrapped in the NPs, tau 4 ns, shown in green), and local overlap of both (turquoise tones) was visualized in the red fluorescence channel *via* FLIM microscopy after simultaneous excitation at 485 nm and 640 nm.

The drug-loaded NPs were incubated with the ROS-producing cells and with HF cells for 24 up to 72 h. Both NPs were at all times more toxic than the free drug (Fig. S17 and S19, *vide* Appendix, **publication 6**), which is generally attributed to the fact that the vast majority of freely administered drug molecules are binding to serum proteins. [256] Tests after 24 h and 48 h comparing PC3, HeLa and HF cells showed a roughly similar toxicity of P-1 and P-2 based NPs in the cancer cells (Fig. S17, *vide* Appendix, **publication 6**). In HF cells the ROS-responsive NPs caused a similar if not slightly lower toxicity than the P-2 NPs (Fig. S17a and S17c, *vide* Appendix, **publication 6**). Cytotoxicity of the polymer itself may be neglected at the concentrations used (Fig. S18, *vide* Appendix, **publication 6**). As another test in HeLa cells had confirmed that particle toxicity steeply increases with incubation time (raised from 12 h to 96 in HeLa cells, Fig. S19, *vide* Appendix, **publication 6**), the difference in toxicity of P-1 and P-2 NPs could become more significant after longer incubation times *e.g.* under conditions of extensive ROS-triggered NPs degradation. Therefore the cancer cells PC3, HeLa and DLD1 were incubated for 72h with P-1 and P-2 NPs, and in addition to standard cell culture conditions a second test with NPs incubated in a medium with a low serum content of 2% was performed (Fig. 35).

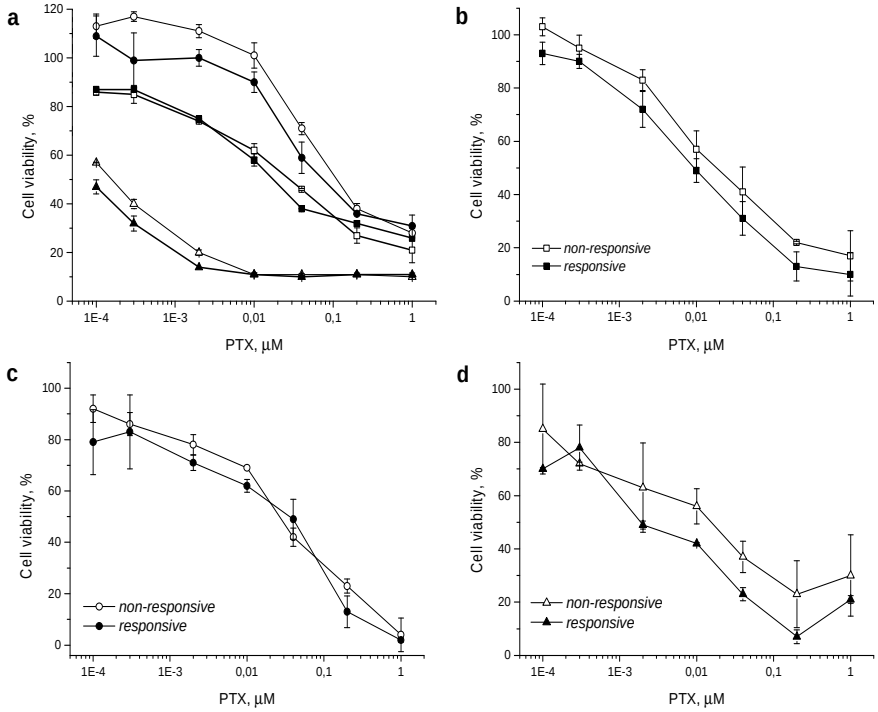

Figure 35. Incubation of PTX-loaded ROS-responsive P-1 (filled marker) and non-responsive P-2 (hollow marker) particles with PC3 (square), DLD1 (circle) and HeLa (triangle) cells for 72h in medium with 10% serum (a). Similar testing was done in medium with only 2% of serum, comparing again the cell lines PC-3 (b), DLD1 (c) and HeLa (d) cells after 72h incubation.

Reducing the serum content in the incubation medium is known to increase the overall uptake rate of NPs, [257] (as also observed by the authors, unpublished data), which in return might enhance the superior toxicity of P-1 NPs for cancer cells. It was found that the lower serum content caused no additional damage to the cells in Alamar Blue® assay (data not shown). In all three cancer cell lines including the experiments in medium with 2% and with 10% serum content, the toxicity of the responsive P-1 NPs was slightly higher than that of non-responsive P-2 NPs. The viability testing demonstrated herein that under the studied conditions the PTX-loaded ROS-responsive NPs appear more cytotoxic in tumor cells than their non-responsive counterpart NPs (Fig. 35).

In summary, we have shown evidence that fluorescent polymer NPs, bearing pinacol-type boronic ester linkers trigger self-immolative polymer degradation and subsequently release the cargo drug in the presence of ROS concentrations typically present in intracellular environment of certain tumor cells. Co-localization studies evidenced that the P-1 polymer NPs can be used for selective cargo release to PC3 cancer cells, with the release rate in non-cancer HF cells being lower. Finally the drug-loaded ROS-responsive NPs were shown to be more cytotoxic to tumor cells compared to their non-responsive counterparts making the presented polymer a promising candidate for applications as delivery system and imaging agent (theranostics) aimed at inflamed microenvironments and cancer tissue.

5. Conclusions

This thesis has focused on the potential and current uses of soft matter based nanomedicines in cancer therapies. After a brief overview of the current status (clinical trials and marketed products) of successful cases as well as main advantages and drawbacks of soft matter formulations, several responsive and non-responsive soft matter assemblies (polymer NPs and block copolymer NPs) were synthesized, discussed and presented. We demonstrated the efficacy of the combination chemotherapy in comparison to single NP-loaded drugs in *in vivo* experiments from novel biodegradable/biocompatible non-responsive (PBSBDL copolymer) NPs loaded with doxorubicin or docetaxel. In *in vitro* cytotoxicity studies the novel pH-responsive block copolymer (MPEO-*b*-PCL block copolymer) NPs containing ketal groups as block linkers and loaded with paclitaxel showed an important increase in activity compared to the free drug. Furthermore, the former NPs were degraded into well-known and FDA-approved by-products that introduce no toxicity to cells. Also in *in vitro* experiments the potential of block copolymer NPs containing fine tunable pH-responsive property of the hydrophobic PDPA core and the protein repellence of the hydrophilic PHPMA shell was demonstrated for the first time. The PHPMA chains prevented the fouling of proteins resulting in a remarkable stability of the NPs in serum and on decreasing pH the hydrophobic PDPA block becomes protonated (hydrophilised) in the narrow range of pH ($6.51 < pH < 6.85$; $\Delta pH \sim 0.34$) resulting in the fast disassembly of the NPs and chemotherapeutic drug release in model cancer cells. Finally, a biocompatible/biodegradable ROS-responsive soft matter assemble was prepared for drug delivery and imaging of ROS-rich environments. *In vitro* data proved that the presented polymer system released more the model drug in comparison to a polymer counterpart as well as specifically and efficiently in cancer cells, while the release in non-cancer cells (HF cells) was low making the presented polymer a potential candidate for applications as delivery system and imaging agent (theranostics) aimed at specifically inflamed and/or cancer cells. The recent advances in soft matter based nanomedicines, as reported in this thesis, suggest a bright future for further scientific investigations of innovative soft therapeutics into clinical practice.

6. References

[1] World Health Organization (WHO). http://www.who.int/mediacentre/news/releases/2006/pr06/en/ (July, 2014).

[2] Griffioen, A.W.; Molema, G. *Pharmacol. Rev.*, **2000**, *52*, 237-268.

[3] Fang, J.; Nakamura, H.; Maeda, H. *Adv. Drug Del. Rev.*, **2011**, *63*, 136-151.

[4] Chiche, J.; Brahimi-Horn, M.C.; Pouysségur, J. *J. Cell Mol. Med.*, **2010**, *14*, 771-794.

[5] van Sluis, R.; Bhujwalla, Z.M.; Raghunand, N.; Ballesteros, P.; Alvarez, J.; Cerdan, S.; Galons, R.J.; Gillies, R.J. *Magn. Reson. Med.*, **1999**, *41*, 743-750.

[6] Cardone, R.A.; Casavola, V.; Reshkin, S.J. *Nat. Rev. Cancer*, **2005**, *5*, 786-795.

[7] Binauld, S.; Stenzel, M.H. *Chem. Commun.*, **2013**, *49*, 2082-2102.

[8] Ko, J.; Park, K.; Kim, Y.-S.; Kim, M.S.; Han, J.K.; Kim, K.; Park, R-W.; Kim, I.-S.; Song, H.K.; Lee, D.S., Kwon, I.C. *J. Control. Release*, **2007**, *123*, 109-115.

[9] Chen, W.; Meng, F.; Li, F.; Ji, S.-J.; Zhong, Z. *Biomacromolecules*, **2009**, *10*, 1727-1735.

[10] Petrova, S.; Jäger, E.; Konefał, R.; Venturini, C.G.; Spěváček, J.; Pavlova, E.; Štěpánek, P. *Polym. Chem.*, **2014**, *5*, 3884-3893.

[11] Jain, R.K.; Stylianopoulos, T. *Nat. Rev. Clin. Oncol.*, **2010**, *7*, 653-664.

[12] Ruenraroengsak, P.; Cook, J.M.; Florence, A.T. *J. Control. Release*, **2010**, *141*, 265-276.

[13] Cho, K.; Wang, X.; Nie, S.; Chen, Z.; Shin, D.M. *Clin. Cancer Res.*, **2008**, *14*, 1310-1316.

[14] Brown J.M.; Giaccia, A.J. *Cancer Res.*, **1998**, *58*, 1408-1416.

[15] Chauhan, V.P.; Jain, R.K. *Nat. Mater.*, **2014**, *12*, 958-962.

[16] Gerlowski, L.E.; Jain, R.K. *Microvasc. Res.*, **1986**, *31*, 288-305.

[17] Matsumura, Y.; Maeda, H. *Cancer Res.*, **1986**, *46*, 6387-6392.

[18] Hobbs, S.K.; Monsky, W.L.; Yuan, F.; Roberts, W.G.; Griffith, L.; Torchilin, V.P.; Jain, R.K. *Proc. Natl. Acad. Sci. U.S.A*, **1998**, *95*, 4607-4612.

[19] Yuan, F.; Dellian, M.; Fukumura, D.; Leunig, M.; Berk, D.A.; Torchilin. V.P.; Jain, R.K. *Cancer Res.*, **1995**, *55*, 3752-3756.

[20] Danhier, F.; Feron, O.; Preát, V. *J. Control. Release*, **2010**, *148*, 135-146.

[21] Fang, J.; Nakamura, H.; Maeda, H. *Adv. Drug Del. Rev.*, **2011**, *63*, 136-151.

[22] Maeda, H.; Matsumura, Y. *Crit. Rev. Ther. Drug Carrier Syst.*, **1989**, *6*, 193-210.

[23] Maeda, H.; Wu, J.; Sawa, T.; Matsumura, Y.; Hori, K. *J. Control. Release*, **2000**, *65*, 271-284.

[24] Torchilin, V. *Adv. Drug. Deliv. Rev.*, **2011**, *63*, 131-135.

[25] Lammers, T.; Kiessling, F.; Hennink, W.E.; Storm, G. *J. Control. Release*, **2012**, *161*, 175-187.

[26] Bae, Y.H.; Park, K. *J. Control. Release*, **2011**, *153*, 198-205.

[27] Fukumura, D.; Yuan, F.; Monsky, W.L.; Chen, Y.; Jain, R.K. *Am. J. Pathol.*, **1997**, *151*, 679-688.

[28] Monsky, W.L.; Mouta Carreira, C.; Tsuzuki, Y.; Gohongi, T.; Fukumura, D.; Jain, R.K. *Clin. Cancer Res.*, **2002**, *8*, 1008-1013.

[29] Prabhakar, U.; Maeda. H.; Jain. R.K.; Sevick-Muraca, E.M.; Zamboni, W.; Farokhzad, O.C.; Barry, S.T.; Gabizon, A.; Grodzinski, P.; Blakey, D.C. *Cancer Res.*, **2013**, *73*, 2412-2417.

[30] Bertrand, N.; Wu, J.; Xu, X.; Kamaly, N.; Farokhzad, O.C. *Adv. Drug Del. Rev.*, **2014**, *66*, 2-25.

[31] Kirpotin D.B, Drummond D.C, Shao Y, Shalaby M.R., Hong K, Nielsen U.B., Marks J.D., Benz C.C., Park J.W. *Cancer Res.*, **2006**, *66*, 6732-6740.

[32] Choi C.H.J., Alabi C.A., Webster P., Davis M.E. *Proc. Natl. Acad. Sci U.S.A*, **2010**, *107*, 1235-1240.

[33] van der Meel, R.; Vehmeijer L.J.C.; Kok R.J.; Storm, G.; van Gaal E.V.B. *Adv. Drug Del. Rev.*, **2013**, *65*, 1284-1298.

[34] Ruoslahti, E.; Bhatia, S.N.; Sailor M.J. *J. Cell Biol.* **2010**, *188*, 759-768.

[35] Dominska, M.; Dykxhoorn, D.M. *J. Cell Sci.*, **2010**, *123*, 1183-1189.

[36] Hatakeyama, H.; Akita, H.; Ishida, E.; Hashimoto, K.; Kobayashi, H.; Aoki, T.; Yasuda, J.; Obata, K.; Kikuchi, H.; Ishida, T.; Kiwada, H.; Harashima, H. *Int. J. Pharm.*, **2007**, *342*, 194-200.

[37] Morachis, J.M.; Mahmoud, E.A.; Almutairi, A. *Pharmacol. Rev.*, **2012**, *64*, 505-519.

[38] Elias, D.R.; Poloukhtine, A.; Popik, V.; Tsourkas, A. *Nanomedicine*, **2013**, *9*, 194-201.

[39] Gao, H.; Yang, Z.; Zhang, S.; Cao, S.; Shen, S.; Pang, Z.; Jiang, X. *Sci. Rep.*, **2013**, *3*, 2534.

[40] Ke, W.; Shao, K.; Huang, R.; Han, L.; Liu, Y.; Li, J.; Kuang, Y.; Ye, L.; Lou, J.; Jiang, C. *Biomaterials*, **2009**, *30*, 6976-6985.

[42] Mura, S.; Nicolas, J.; Couvreur, P. *Nat. Mater.*, **2013**, *12*, 991-1003.

[43] Sahay, G.; Alakhova, D.Y.; Kabanov, A.V. *J. Control. Release*, **2010**, *145*, 182-195.

[44] Wei, H.; Zhuo, R.-X.; Zhang, X.-Z. *Prog. Pol. Sci.*, **2013**, *38*, 503-535.

[45] Bangham, A.D.; Standish, M.M.; Watkins, J.C. *J. Mol. Biol.*, **1965**, *13*, 238-252.

[46] Deamer, D.W. *FASEB J.*, **2010**, *24*, 1308-1310.

[47] Allen, T.M.; Cullis, P.R. *Adv. Drug Del. Rev.*, **2013**, *65*, 36-48.

[48] Torchilin, V.P. *Nat. Rev. Drug Discov.*, **2005**, *4*, 145-160.

[49] Duncan, R. *Nat. Rev. Drug. Discov.*, **2003**, *2*, 347-360.

[50] Kohli, A.G.; Kierstead, P.H.; Venditto, V.J.; Walsh, C.L.; Szoka, F.C. *J. Control. Release*, **2014**, 190, 274-287.

[51] Ozpolat, B.; Sood, A.K.; Lopez-Berestein, G. *Adv. Drug Del. Rev.*, **2014**, *66*, 110-116.

[52] Couvreur, P. *Adv. Drug Del. Rev.*, **2013**, *65*, 21-23.

[53] Marty, J.J.; Oppenheim, R.C.; Speiser, P. *Pharm. Acta Helv.*, **1978**, *53*, 17-23.

[54] Illum, L.; Jones, P.D.; Baldwin, R.W.; Davis, S.S. *J. Pharmacol. Exp. Ther.*, **1984**, *230*, 733-736.

[55] Jalil, R.-U. *Drug Dev. Ind. Pharm.*, **1990**, *16*, 2353-2367.

[56] Heller, J. *Crit. Rev. Ther. Drug.*, **1984**, *1*, 39-90.

[57] Gurny, R.; Peppas, N.A.; Harrington, D.D.; Banker, G.S. *Drug Dev. Ind. Pharm.*, **1981**, *7*, 1-25.

[58] Calvo, P.; Remuñán-López, C.; Vila-Jato, J.L.; Alonso, M.J. *J. Appl. Polym. Sci.*, **1997**, *63*, 125-132.

[59] Soppimath, K.S.; Aminabhavi, T.M.; Kulkarni, A.R.; Rudzinski, W.E. *J. Control. Release*, **2001**, *70*, 1-20.

[60] Fessi, H.; Puisieux, F.; Devissaguet, J.-Ph.; Ammoury, N.; Benita, S. *Int. J. Pharm.*, **1984**, *55*, R1-R4.

[61] Quintanar-Guerrero, D.; Allémann, E.; Fessi, H.; Doelker, E. *Drug Dev. Ind. Pharm.*, **1998**, *24*, 1113-1128.

[62] Karnik R.; Gu F.; Basto, P.; Cannizzaro, C.; Dean, L.; Kyei-Manu, W.; Langer, R.; Farokhzad, O.C. *Nano Lett.*, **2008**, *8*, 2906-2912.

[63] Rolland, J.P. Maynor, B.W.; Euliss, L.E.; Exner, A.E.; Denison, G.M.; DeSimone, J.M. *J. Am. Chem. Soc.*, **2005**, *127*, 10096-10100.

[64] Enlow, E.M.; Luft, J.C.; Napier, M.E.; Desimone, J.M. *Nano Lett.*, **2011**, *11*, 808-813.

[65] Chu, K.S.; Hasan, W.; Rawal, S.; Walsh, M.D.; Enlow, E.M.; Luft, J.C.; Bridges, A.S.; Kuijer, J.L.; Napier, M.E.; Zamboni, W.C.; DeSimone, J.M. *Nanomedicine*, **2013**, *9*, 686-693.

[66] Gaucher, G.; Robert H. Marchessault, R.H.; Leroux, J.-C. *J. Control. Release*, **2010**, *143*, 2-12.

[67] Tong, R.; Gabrielson N.P.; Fan, T.M.; Cheng, J. *Curr. Opin. Solid State Mater. Sci.*, **2012**, *16*, 323-332.

[68] Weiss, V.M.; Naolou, T.; Hause, G.; Kuntsche, J.; Kressler, J.; Mäder, K. *J. Control. Release*, **2012**, *158*, 156-164.

[69] Jäger, A.; Gromadzki, D.; Jäger, E.; Giacomelli, F.C.; Kozlowska, A.; Kobera, L.; Brus, J.; Říhová, B.; El Fray, M.; Ulbrich, K.; Štěpánek, P. *Soft Matter*, **2012**, *8*, 4343-4354.

[70] Lemarchand, C.; Gref, R.; Passirani, C.; Garcion, E.; Petri, B.; Müller, R.; Costantini, D.; Couvreur, P. *Biomaterials*, **2006**, *27*, 101-118.

[71] Rudt, S.; Müller, R.H. *J. Control. Release*, **1993**, *25*, 51-59.

[72] Sahho, S.K.; Panyam, J.; Prabha, S.; Labhasetwar, V. *J. Control. Release*, **2002**, *82*, 105-114.

[73] Roosjen, A.; de Vries, J.; van der Mei, H.C.; Norde, W.; Busscher, H. *J. Biomed. Mater. Res. Part B*, **2005**, *73B*, 347-354.

[74] Branch, D.W.; Wheeler, B.C.; Brewer, G.J.; Leckband, D.E. *Biomaterials*, **2001**, *22*, 1035-1047.

[75] Rodriguez-Emmeneger, C.; Jäger, A.; Jäger, E.; Štěpánek, P. Bollogna-Alles, A.; Guterres, S.S.; Pohlmann, A.R.; Brynda, E. *Colloids Surf. B*, **2011**, *83*, 376-381.

[76] Feng, S.-S.; Mu, L.; Win, K.Y.; Huang, G. *Curr. Med. Chem.*, **2004**, *11*, 413-424.

[77] Win, K.Y.; Feng, S.-S. *Biomaterials*, **2005**, *26*, 2713-2722.

[78] Feng, S.-S.; Zhao, L.; Zhang, Z.; Bhakta, G.; Win, K.Y.; Dong, Y.; Chien, S. *Chem. Eng. Sci.*, **2007**, *62*, 6641-6648.

[79] Zhao, L.; Feng, S.-S. *J. Pharm. Sci.*, **2010**, *99*, 3552-3560.

[80] Jäger, E.; Jäger, A.; Etrych, T.; Giacomelli, F.C.; Chytil, P.; Jigounov, A.; Putaux, J.-L.; Říhová, B.; Ulbrich, K.; Štěpánek, P. *Soft Matter*, **2012**, *8*, 9563-9575.

[81] Jäger, E.; Jäger, A.; Chytil, P.; Etrych, T.; Říhová, B.; Giacomelli, F.C.; Štěpánek, P.; Ulbrich, K. *J. Control. Release*, **2013**, *165*, 153-161.

[82] Tuzar, Z.; Kratochvil, P. *Adv. Colloid Interface Sci.*, **1976**, *6*, 201-232.

[83] Kataoka, K.; Harada, A.; Nagasaki, Y. *Adv. Drug Del. Rev.*, **2001**, *47*, 113-131.

[84] Torchilin, V.P. *Pharm. Res.*, **2007**, *24*, 1-16.

[85] Nishiyyama, N.; Kataoka, K. *Pharmacol. Ther.*, **2006**, *112*, 630-648.

[86] Rapoport, N.; *Prog. Pol. Sci.*, **2007**, *32*, 962-990.

[87] Schmaljohann, D. *Adv. Drug. Del. Rev.*, **2006**, *58*, 1655-1670.

[88] Giacomelli, F.C.; Štěpánek, P.; Giacomelli, C.; Schmidt, V.; Jäger, E.; Jäger, A.; Ulbrich, K. *Soft Matter*, **2011**, *7*, 9316-9325.

[89] Pegoraro, C.; Cecchin, D.; Gracia, L.S.; Warren, N.; Madsen, J.; Armes, S.P.; Lewis, A.; MacNeil, S.; Battaglia, G. *Cancer Lett.*, **2013**, *334*, 328-337.

[90] Wang, Y.; Zhou, K.; Huang, G.; Hensley, C.; Huang, X.; Ma, X.; Zhao, T.; Sumer, B.D.; DeBerardinis, R.J.; Gao, J. *Nat. Mater.*, **2014**, *13*, 204-212.

[91] Lavasanifar, A.; Samuel, J.; Kown, G.S. *Adv. Drug Del. Rev.*, **2002**, *54*, 169-190.

[92] Osada, K.; Christie, R.J.; Kataoka, K. *J. R. Soc. Interface*, **2009**, *6*, S325-S339.

[93] Duncan, R. *Nat. Rev. Cancer*, **2006**, *6*, 688-701.

[94] Kopeček, J. *Adv. Drug Del. Rev.*, **2013**, *65*, 49-59.

[95] Yang, J.; Kopeček, J. *J. Control. Release*, **2014**, 190, 288-303.

[96] Duncan, R.; Vicent, M.J. *Adv. Drug Del. Rev.*, **2013**, *65*, 60-70.

[97] Ulbrich, K.; Subr, V. *Adv. Drug Del. Rev.*, **2004**, *56*, 1023-1050.

[98] Choi, W.M.; Kopečekova, P.; Minko, T.; Kopeček, J. *J. Bioact. Compat. Polym.*, **1999**, *14*, 447-456.

[99] Etrych, T. Jelínkova, M.; Říhová, B.; Ulbrich, K. *J. Control. Release*, **2001**, *73*, 89-102.

[100] Murthy, N.; Campbell, J.; Fausto, N.; Hoffman, A.S.; Stayton, P.S. *J. Control. Release*, **2003**, *89*, 365-374.

[101] Veronese, F.M.; Schiavon, O.; Pasut, G.; Mendichi, R.; Andersson, L.; Tsirk, A.; Ford, J.; Wu, G.; Kneller, S.; Davies, J.; Duncan, R. *Bioconjugate Chem.*, **2005**, *16*, 775-784.

[102] Blencowe, C.A.; Russel, A.T.; Greco, F.; Hayes, W.; Thornthwaite, D.W. *Polym. Chem.*, **2011**, *2*, 773-790.

[103] Li, W.; Zhan, P.; De Clerq, E.; Lou, H.; Liu, X. *Prog. Pol. Sci.*, **2013**, *38*, 421-444.

[104] Veronese, F.M.; Pasut, G. *Drug Discov. Today*, **2005**, *10*, 1451-1458.

[105] Etrych, T.; Šubr, V.; Strohalm, J.; Šírová, M.; Říhová, B.; Ulbrich, K. *J. Control. Release*, **2012**, *164*, 346-354.

[106] Pan, H.; Sima, M.; Yang, J.; Kopeček, J. *Macromol. Biosci.*, **2013**, *13*, 155-160.

[107] Roberts, M.J.; Bentley, M.D.; Harris, J.M. *Adv. Drug Del. Rev.*, **2002**, *54*, 459-476.

[108] Pang, X.; Du, H.-L.; Zhang, H.-Q.; Zhai, Y.-J.; Zhai, G.-X. *Drug Discov. Today*, **2013**, *18*, 1316-1322.

[109] Pola, R.; Studenovský, M.; Pechar, M.; Ulbrich, K.; Hovorka, O.; Větvička, D.; Říhová, B. *J. Drug Target.*, **2009**, *17*, 763-776.

[110] Etrych, T.; Strohalm, J.; Kovář, L.; Kabešová, M.; Říhová, B.; Ulbrich, K. *J. Control. Release*, **2009**, *140*, 18-26.

[111] Ulbrich, K.; Šubr, V. *Adv. Drug Del. Rev.*, **2010**, *62*, 150-166.

[112] Etrych, T.; Šubr, V.; Laga, R.; Říhová, B.; Ulbrich, K. *Eur. J. Pharm. Sci.*, **2014**, *58*, 1-12.

[113] Vicent, M.J.; Greco, F.; Nicholson, R.I.; Paul, A.; Griffiths, P.C.; Duncan, R. *Angew. Chem. Int. Ed.*, **2005**, *44*, 4061-4066.

[114] Kostkova, H.; Etrych, T.; Říhova, B.; Ulbrich, K. *J. Biocom. Bioconj. Pol.*, **2011**, *26*, 270-286.

[115] Lammers, T.; Šubr, V.; Ulbrich, K.; Peschke, P.; Huber, P.E.; Hennink, W.E.; Storm, G. *Biomaterials*, **2009**, *30*, 3466-3475.

[116] Kostkova, H.; Etrych, T.; Říhova, B.; Koskta, L.; Starovoytova, L.; Kovar, M.; Ulbrich, K. *Macromol. Biosci.*, **2013**, *13*, 1648-1660.

[117] Zhang, R.; Luo, K.; Yang, J.; Sima, M.; Sun, Y.; Janát-Amsbury, M.M.; Kopeček, J. *J. Control. Release*, **2013**, *166*, 66-74.

[118] Li, C.; Wallace, S. *Adv. Drug Del. Rev.*, **2008**, *60*, 886-898.

[119] http://clinicaltrials.gov/show/NCT01655693 (June, 2014)

[120] Barraud, L.; Merle, P.; Soma, E.; Lefrançois, L.; Guerret, S.; Chevallier, M.; Dubernet, C.; Couvreur, P.; Trépo, C.; Vitvitski, L. *J. Hepatol.*, **2005**, *42*, 736-743.

[121] Merle, P.; Ahmed, S.Si.; Habersetzer, F.; Abergel, A.; Taieb, J.; Bonyhay, L.; Costantini, D.; Dufour-Lamartinie, J.; Trepo, C. *J. Clin. Oncol.*, **2006**, *24*, 14094.

[122] www.BioAlliancePharma.com (July 2014)

[123] http://clinicaltrials.gov/show/NCT01655693 (June 2014).

[124] Zhang, Z.; Liao, G.; Nagai, T.; Hou, S. *Int. J. Pharm.*, **1996**, *139*, 1-8.

[125] Zhou, Q.; Sun, X.; Zeng, L.; Liu, J.; Zhang, Z. *Nanomedicine*, **2009**, *5*, 419-426.

[126] Lu, Y.; Park, K. *Int. J. Pharm.*, **2013**, *453*, 198-214.

[127] Cabral, H.; Kataoka, K. *J. Control. Release*, **2014**, DOI: 10.1016/j.jconrel.2014.06.042.

[128] Lee, K.S.; Chung, H.C.; Im, S.A.; Park, Y.H.; Kim, C.S.; Kim, S.B.; Rha, S.Y.; Lee, M.Y.; Ro, J. *Breast Cancer Res. Treat.*, **2008**, *108*, 241-250.

[129] Kim, D.-W.; Kim, S.-Y.; Kim, H.-K.; Kim, S.-W.; Shin, S.W.; Kim, J.S.; Park, K.; Lee, M.Y.; Heo, D.S. *Ann. Oncol.*, **2007**, *18*, 2009-2014.

[130] http://clinicaltrials.gov/ct2/show/NCT00912639 (June, 2014)

[131] http://clinicaltrials.gov/ct2/show/NCT01689194 (June, 2014)

[132] Kato, K.; Chin, K.; Yoshikawa, T.; Yamaguchi, K.; Tsuji, Y.; Esaki, T.; Sakai, K.; Kimura, M.; Hamaguchi, T.; Shimada, Y.; Matsumara, Y.; Ikeda, R. *Invest. New Drugs*, **2012**, *30*, 1621-1627.

[133] http://clinicaltrials.gov/ct2/show/NCT01644890 (June, 2014)

[134] Nishiyama, N.; Okazaki, S.; Cabral, H.; Miyamoto, M.; Kato, Y.; Sugiyama, Y.; Nishio, K.; Matsumura, Y.; Kataoka, K. *Cancer Res.*, **2003**, *63*, 8977-8983.

[135] Plummer, R.; Wilson, R.H.; Calvert, H.; Boddy, A.V.; Griffin, M.; Sludden, J.; Tilby, M.J.; Eatock, M.; Pearson, D.G.; Ottley, C.J.; Matsumura, Y.; Kataoka, K.; Nishiya, T. *Brit. J. Cancer*, **2011**, *104*, 593-598.

[136] http://clinicaltrials.gov/ct2/show/NCT02043288 (June, 2014)

[137] Matsumura, Y. *Adv. Drug Del. Rev.*, **2011**, *63*, 184-192.

[138] http://clinicaltrials.gov/ct2/show/NCT00951054 (June, 2014)

[139] http://clinicaltrials.gov/ct2/show/NCT01238939 (June, 2014)

[140] Matsumura, Y.; Hamaguchi, T.; Ura, T.; Muro, K.; Yamada, Y.; Shimada, Y.; Shirao, K.; Okusaka, T.; Ueno, H.; Ikeda, M.; Watanabe, W. *Br. J. Cancer*, **2004**, *91*, 1775-1781.

[141] Harada, M.; Bobe, I.; Saito, H.; Shibata, N.; Tanaka, R.; Hayashi, T.; Kato, Y. *Cancer Sci.*, **2011**, *102*, 192-199.

[142] Takahashi, A.; Yamamoto, Y.; Yasunaga, M.; Koga, Y.; Kuroda, J.-I.; Takigahira, M.; Harada, M.; Saito, H.; Hayashi, T.; Kato, Y.; Kinishita, T.; Ohkohchi, N.; Hyodo, I.; Matsumura, Y. *Cancer Sci.*, **2013**, *104*, 920-925.

[143] Matsumura, Y. *Jpn. J. Clin. Oncol.*, **2014**, *44*, 515-525.

[144] Alakhov, V.; Klinski, E.; Li, S.; Pietrzynski, G.; Venne, A.; Batrakova, E.; Bronitch, T.; Kabanov, A. *Colloids Surf. B*, **1999**, *16*, 113-134.

[145] Danson, S.; Ferry, D.; Alakhov, V.; Margison, J.; Kerr, D.; Jowle, D.; Brampton, M.; Halbert, G.; Ranson, M. *Br. J. Cancer*, **2004**, *90*, 2085-2091.

[146] Valle, J.W.; Armstrong, A.; Newman, C.; Alakhov, V.; Pietrzynski, G.; Brewer, J.; Campbell, S.; Corrie, P.; Rowinsky, E.K.; Ranson, M. *Invest. New Drugs*, **2011**, *5*, 1029-1037.

[147] http://clinicaltrials.gov/ct2/show/NCT01300533 (June, 2014)

[148] http://clinicaltrials.gov/ct2/show/NCT01812746 (June, 2014)

[149] Owen, S.C.; Cahn, D.P.Y.; Shoichet, M.S. Nano Today, 2012, 7, 53-65.

[150] Talelli, M.; Iman, M.; Varkouhi, A.K.; Rijcken, C.J.F.; Schiffelers, R.M.; Etrych, T.; Ulbrich, K.; van Nostrun, C.F.; Lammers, T.; Storm, G.; Hennink, W.E. *Biomaterials*, **2010**, *31*, 7797-7804.

[151] Cho, E.C.; Zhang, Q.; Xia, Y.N. *Nat. Nanotechnol.*, **2011**, *6*, 385-391.

[152] Dawidczyk, C.M.; Kim, C.; Park, J.H.; Russel, L.M.; Lee, K.H.; Pomper, M.G.; Searson, P.C. *J. Control. Release*, **2014**, *187*, 133-144.

[153] Gabizon, A.; Shmeeda, H.; Barenholz, Y. *Clin. Pharmakokinetics*, **2003**, *42*, 419-436.

[154] Uchiyama, K.; Nagayasu, A.; Yamagiwa, Y.; Nishida, T.; Harashima, H.; Kiwada, H. *Int. J. Pharm.*, **1995**, *121*, 195-203.

[155] Cabral, H.; Matsumoto, Y.; Mizuno, K.; Chen, Q.; Murakami, M.; Kimura, M.; Terada, Y.; Kataoka, K. *Nat. Nanotechnol.*, **2011**, *6*, 815-823.

[156] Fox, M.E.; Szoka, F.C.; Fréchet, J.M.J. *Acc. Chem. Res.*, **2009**, *42*, 1141-1151.

[157] Owens, D.E.; Peppas, N.A. *Int. J. Pharm.*, **2006**, *307*, 93-102.

[158] Dobrovolskaia, M.A.; Aggarwal, P.; Hall, J.B.; McNeil, S.E. *Mol. Pharm.*, **2008**, *5*, 487-495.

[159] Gratton, S.E.A.; Ropp, P.A.; Pohlhaus, P.D.; Luft, J.C.; Madden, V.J.; Napier, M.E.; DeSimone, J.M. *Proc. Natl. Acad. Sci. U.S.A.*, **2008**, *105*, 11613-11618.

[160] He, C.; Hu, Y.; Yin, L.; Tang, C.; Yin, C. *Biomaterials*, **2010**, *31*, 3657-3666.

[161] Xiao, K.; Li, Y.; Luo, J.; Lee, J.C.; Xiao, W.; Gonik, A.M.; Agarwal, R.G.; Lam, K.S. *Biomaterials*, **2011**, *32*, 3435-3446.

[162] Zhu, M.; Nie, G.; Meng, H.; Xia, T.; Nel, A.; Zhao, Y. *Acc. Chem. Res.*, **2013**, *46*, 622-631.

[163] Mu, Q.; Jaing, G.; Chen, L.; Zhou, H.; Fourches, D.; Tropsha, A.; Yan, B. *Chem. Rev.*, **2014**, 114, 7740-7781.

[164] Geng, Y.; Dalhaimer, P.; Cai, s.; Tsai, R.; Tewari, M.; Minko, T.; Discher, D.E. *Nat. Nanotech.*, **2007**, *2*, 249-255.

[165] Choi, H.S.; Liu, W.; Misra, P.; Tanaka, E.; Zimmer, J.P.; Ipe, B.I.; Bawendi, M.G.; Frangioni, J.V. *Nat. Biotechnol.*, **2007**, *25*, 1165-1170.

[166] Longmire, M.; Choyke, P.L.; Kobayashi, H. *Nanomedicine*, **2008**, *3*, 703-717.

[167] Maeda, H.; Nakamura, H.; Fang, J. *Adv. Drug Del. Rev.*, **2013**, *65*, 71-79.

[168] Koning, G.A.; Fretz, M.M.; Woroniecka, U.; Storm, G.; Krijger, G.C. *Appl. Radiat. Isot.*, **2004**, *61*, 963-967.

[169] Chou, L. Y.T.; Ming, K.; Chan, W.C.W. *Chem. Soc. Rev.*, **2011**, *40*, 233-245.

[170] Lin, C-A.J.; Sperling, R.A.; Li, J.K.; Yang, T-Y.; Li, P-Y.; Zanella, M.; Chang, W.H.; Parak, W.J. *Small*, **2008**, *4*, 334-341.

[171] Euliss, L.E.; DuPont, J.A.; Gratton, S.; DeSimone, J. *Chem. Soc. Rev.*, **2006**, *35*, 1095-1104.

[172] Ha, C. S.; Gardella, J. A. Jr. Chem. Rev., **2005**, *105*, 4205-4232.

[173] Schubert, S.; Delaney, J.T.Jr.; Schubert, U.S. *Soft Matter*, **2011**, *7*, 1581-1588.

[174] Campolongo, M. J.; Luo D. Old polymers lern new tracts. *Nat. Mater.*, **2009**, *8*, 447-449.

[175] Anderson, J. M.; Shive, M. S. *Adv. Drug Deliv. Rev.*, **1997**, *28*, 5-24.

[176] Panyam J, Labhasetwar V. *Adv. Drug Deliv. Rev.*, **2003**, *55*, 329-347.

[177] Lindström, A., Alberstsson, A.C., Hakkarainen, M. *Polym. Degrad. Stab.*, **2004**, *83*, 487-493.

[178] Scímeca, J.A. Cancer inhibition in animals. In: Advances in Conjugated Linoleic Acid Research, Vol. 1 (Yurawecz, M.P., Mossobo, M.M., Kramer, J.K.G., Pariza, M.W., Nelson, G.J., eds.), pp. 420-443. AOCS Press, Champaign, IL.

[179] Belury, M.A. *J. Nutr.*, **2002**, *132*, 2995-2998.

[180] Belury, M.A., Vanden Heuvel, J.P. *Nutr. Disease Update* **1997**, *1*, 58-63.

[181] Belury, M.A., Mahon, A., Banni, S. *J. Nutr.*, **2003**, *133*, 257S-260S.

[182] Paton, C.M., Ntambi, J.M. *AJP-Endocrinol. Metab.*, **2009**, *297*, E28-E37.

[183] El Fray, M. *Adv. Eng. Mater.*, **2009**, *11*, B35-40.

[184] El-Fray, M.; Piegat, A.; Prowans, P. *Adv. Eng. Mater.*, **2009**, *11*, B200-203.

[185] Domb, A., J.; Maniar, M. *J. Polym. Sci. Part A Polym. Chem.*, **1993**, *31*, 1275-1285.

[186] Prowansa, P.; El Fray, M.; Slonecki, J. *Biomaterials*, **2002**, *23*, 2973-2978.

[187] Renke-Gluszko, M.; El Fray, M. *Biomaterials*, **2004**, *25*, 5191-5198.

[188] El Fray, M.; Feldmann, M.; Ziegler, G.; Prowans, P. *J. Mater. Sci*: *Mater. Med.*, **2007**, *18*, 501-506.

[189] Meng, F. H.; Zhong, Z.Y.; Feijen, J. *Biomacromolecules* **2009**, *10*, 197-209.

[190] Fattal, E.; Couvreur, P.; Dubernet, C. *Adv. Drug Deliver. Rev.*, **2004**, *56*, 931-946.

[191] C.D.H Alarcon, S. Pennadam, C. Alexander, *Chem. Soc. Rev.*, **2005**, *34*, 276-285.

[192] Kelley, E.G.; Albert, J. N. L.; Sullivan, M. O.; Epps III, T. H. *Chem. Soc. Rev.*, **2013**, *42*, 7057-7071.

[193] Fleige, E.; Quadir, M.A.; Haag, R. *Adv. Drug Deliver. Rev.*, **2012**, *64*, 866-884.

[194] Schmaljohann, D. *Adv. Drug Deliver. Rev.*, **2006**, *58*, 1655-1670.

[195] Vaupel, P.; Kallinowski, F.; Okunieff, P. *Cancer Res.*, **1989**, *49*, 6449-6465.

[196] Mukherjee, S.; Ghosh, R.N.; Maxfield, F.R. *Endocytosis, Physiol. Rev.*, **1997**, *77*, 759-803.

[197] Wilson, D.S., Dalmasso, G., Wang, L., Sitaraman, S.V., Merlin, D., Murthy, N. *Nat. Mater.*, **2010**, *9*, 923-928.

[198] Fomina, N., McFearin, C.L., Almutairi, A. *Chem. Comm.*, **2012**, *48*, 9138-9140.

[199] Ma, N., Li, Y., Xu, H., Wang, Z., Zhang, X. *J. Am. Chem. Soc.*, **2011**, *132*, 442-443.

[200] Allen, B. L., Johnson, J. D., Walker, J. P. *ACS Nano* **2011**, *5*, 5263-5268.

[201] Allen, B. L., Johnson, J. D., Walker, J. P. *ACS Nano* **2011**, *5*, 5263-5268.

[202] Lee, S.H.; Gupta, M.K.; Bang, J.B.; Bae, H.; Sung, H.-J. *Adv. Healthcare Mater*., **2013**, *2*, 908-15.

[203] Song, C.-C.; Du, F.-S.; Li, Z.-C. *J. Mater. Chem. B*., **2014**, *2*, 3413-3426.

[204] Chytil, P.; Etrych, T.; Koňák, Č.; Šírová, M.; Mrkvan, T.; Bouček, J.; Říhová, B.; Ulbrich, K. *J. Control. Release* **2008**, *127*, 121-130.

[205] Giacomelli, F.C.; Štěpánek, P.; Schmidt, V.; Jäger, E.; Jäger, A.; Giacomelli, C. *Nanoscale* **2012**, *4*, 4504-4514.

[206] Meier, M.A.R.; Aerts, S.N.H.; Staal, B.B.P.; Rasa, M.; Schubert, U.S. *Macromol. Rapid Commun*., **2005**, *26*, 1918-1924.

[207] Nicolas, J.; Mura, S.; Brambila, D.; Mackiewicz, N.; Couvreur, P. *Chem. Soc. Rev*., **2013**, *42*, 1147-1235.

[208] Rieger, J.; Dubois, P.; Jérôme, R.; Jérôme, C. *Langmuir*, **2006**, *22*, 7471-7479.

[209] Kumar, N.; Ravikumar, M.N.V.; Domb, A.J. *Adv. Drug Delivery Rev*., **2001**, *53*, 23-44.

[210] de Oliveira, A.M.; Jäger, E.; Jäger, A.; Štěpánek, P.; Giacomelli, F.C. *Colloids Surf., A*, **2013**, *436*, 1092-1102.

[211] Du, Z.-X.; Xu, J.-T.; Fan, Z.-Q. *Macromolecules* **2007**, *40*, 7633-7637.

[212] Schuetz, P.; Greenall, M. J.; Bent, J.; Furzeland, S.; Atkins, D.; Butler, M.F.; McLeishd, T.C.B.; Buzza, D.M.A. *Soft Matter* **2011**, *7*, 749-759.

[213] S. M. Loverde, M. L. Klein and D. E. Discher, *Adv. Mater*., **2012**, *24*, 3823-3830.

[214] Li, D.; Zhang, Y.; Jin, S.; Guo, J.; Gao, H.; Wang, C. *J. Mater. Chem. B.*, **2014**, *2*, 5187.

[215] Sahay, G.; Alakhova, D.Y.; Kabanov, A.V. *J. Control. Release* **2010**, *145*, 182.

[216] Li, G.L.; Liu, J.Y.; Pang, Y.; Wang, R.B.; Mao, L.M.; Yan, D.Y.; Zhu, X.Y. *Biomacromolecules* **2011**, *12*, 2016.

[217] Rodriguez-Emmenegger, C.; Brynda, E.; Riedel, T.; Houska, M.; Šubr, V.; Alles, A.B.; Hasan, E.; Gautrot, J.E.; Huck, W.T.S. *Macromol. Rapid Commun*., **2011**, *32*, 952.

[218] Whiteman, K.R.; Šubr, V.; Ulbrich, K.; Torchilin, V.P. *J. Liposome Res*., **2001**, *11*, 153.

[219] Cho, K.; Wang, X.; Nie, S.; Chen, Z.; Shin, D.M. *Clin. Cancer Res*., **2008**, *14*, 1310.

[220] Liebmann, J.E.; Cook, J.A.; Lipschultz, C.; Teague, D.; Fisher, J.; Mitchell, J.B. *Br. J. Cancer*, **1993**, *68*, 1104.

[221] Peng, X.; Gong, F.; Chen, Y.; Jiang, Y.; Liu, J.; Yu, M.; Zhang, S.; Wang, M.; Xiao, G.; Liao, H. *Cell Death Dis*., **2014**, *5*, e1367.

[222] Danhier, F.; Lecouturier, N.; Vroman, B.; Jerome, C.; Marchand-Brynaert, J.; Feron, O.; Preat, V. *J. Control. Release*, **2009**, *133*, 11.

[223] Gaucher, G.; Marchessault. R.H.; Leroux, J.-C. *J. Control. Release*, **2010**, *143*, 2.

[224] Wu, Y.; Zhou, D.; Qi, Y.; Xie, Z.; Chen, X.; Jing, X.; Huang, Y. *RSC Adv*., **2015**, *5*, 3523.

[225] Cho, H.; Bae, J.; Garripelli, V.K.; Anderson, J.M.; Jun, H.-W.; Jo, S. *Chem. Commun*., **2012**, *48*, 6043.

[226] Chen, H.; He, W.; Guo, Z. *Chem. Commun*., **2014**, *50*, 9714.

[227] Pu, H.-L.; Chiang, W.-L.; Maiti, B.; Liao, Z.-X.; Ho, Y.-X.; Shim, M.S.; Chuang, E.Y.; Xia, Y.; Sung, H.-W. *ACS Nano* **2014**, *8*, 1213.

[228] Lee, D.; Khaja, S.; Velasquez-Castano, J.C.; Dasari, M.; Sun, C.; Petros, J.; Taylor, W.R.; Murphy, N. *Nat. Mater*., **2007**, *10*, 765.

[229] D'Autréaux, B. and Toledano, M.B. *Nat. Rev. Mol. Cell. Bio*., **2007**, *8*, 813.

[230] Mantovani, A.; Allavena, P.; Sica, A.; Balkwill, F. *Nature* **2008**, *454*, 436.

[231] Reuter, S.; Gupta, S.C.; Chaturvedi, M.M.; Aggarwal, B.B. *Free Radic. Biol. Med*., **2010**, *49*, 1603.

[232] Houstis, N.; Rosen, E.D.; Lander, E.S. *Nature* **2006**, *440*, 944.

[233] Uttara, B.; Singh, A.V.; Zamboni, P.; Mahajan, R.T. *Curr. Neuropharmacol*., **2009**, *7*, 65.

[234] Toyokuni, S.; Okamoto, K.; Yodoi, J.; Hiai, H. *FEBS Lett*., **1995**, *358*, 1.

[235] Szatrowski, T.P.; Nathan, C.F. *Cancer Res*., **1991**, *51*, 794.

[236] Liou, G.-Y.; Storz, P. *Free Radic. Res*., **2010**, *44*, 479.

[237] Waris, G.; Ahsan, H. *J. Carcinog*., **2006**, *5*: 14.

[238] Schumacker, P.T. *Cancer Cell* **2006**, *10*, 175.

[239] López-Lázaro, M.; *Cancer Lett*., **2007**, *252*, 1.

[240] Dröge, W. *Physiol. Rev*., **2002**, *82*, 47.

[241] Kumar, B.; Koul, S.; Khandrika, L.; Meacham, R.B.; Koul, H.K. *Cancer Res*., **2008**, *68*, 1777.

[242] Lallana, E.; Tirelli, N. *Macromol. Chem. Phys*., **2013**, *214*, 143.

[243] Lux, C. de G.;Joshi-Barr, S.; Nguyen, T.; Mahmoud, E.; Schopf, E.; Fomina, N.; Almutairi, A. *J. Am. Chem. Soc*., **2012**, *134*, 15758.

[244] Shim, M.S.; Xia, Y. *Angew. Chem. Int. Ed*., **2013**, *52*, 6926.

[245] Mahmoud, E.A.; Sankaranarayanan, J.; Morachis, J.M.; Kim, G.; Almutairi, A. *Bioconjugate Chem*., **2011**, *22*, 1416.

[246] Jeanmaire, D.; Laliturai, J.; Almalik, A.; Carampin, P.; D'Arcy, R.; Lallana, E.; Evans, R.; Winpeny, R.E.P.; Tirelli, N. *Polym. Chem*., **2015**, *5*, 1393.

[247] Savina, A.; Peres, A.; Cebrian, I.; Carmo, N.; Moita, C.; Hacohen, N.; Moita, L.F.; Amigorena, S. *Immunity* **2009**, *30*, 544.

[248] Jäger, E..; Giacomelli, F.C. *Curr. Top. Med. Chem*., **2015**, *15*, 328.

[249] Hu, T.; Wu, C. *Phis. Rev. Lett*., **1996**, *83*, 4105.

[250] Fu, J.; Wu, C. *J. Polym. Sci., Part B*: *Polym. Phys*., **2001**, *39*, 703.

[251] Kumar , B.; koul, S.; Khandrika, L.; Meacham, R.B.; Koul, H.K. *Cancer Res*., **2008**, *68*, 1777.

[252] Martinez-Outschoorn, U.E.; Balliet, R.M.; Lin, Z.; Whitaker-Menezes, D.; Howell, A.; Sotgia, F.; Lisanti, M.P. *Cell Cycle* **2012**, *11*, 4152.

[253] Lisanti, M.P.; Martinez-Outschoorn, U.E.; Lin, Z.; Pavlides, S.; Whitaker-Menezes, D.; Pestell, R.G.; Howel, A.; Sotgia, F. *Cell Cycle* **2011**, *10*, 2440.

[254] Bhimani, R.S.; Troll, W.; Grunberger, D.; Frenkel, K. *Cancer Res*., **1993**, *53*, 4528.

[255] Lluis, J.M.; Buricchi, F.; Chiarugi, P.; Morales, A.; Fernandez-Checa, J.C. *Cancer Res*., **2007**, *67*, 7368.

[256] Smith, D.A.; Di, L.; Kerns, E.H. *Nat. Rev. Drug Discov*., **2010**, *9*, 929.

[257] Baier, G.; Costa, C.; Zeller, A.; Baumann, D.; Sayer, C.; Araujo, P.H. *Macromol. Biosc*., **2011**, *11*, 628.

7. Appendix – Publications 1 to 6